[redacted]

Copy 6
RM L56F19

NACA RM L56F19

NACA

RESEARCH MEMORANDUM

WIND-TUNNEL INVESTIGATION AT LOW SPEED OF EFFECTS OF SIDESLIP ON STATIC LONGITUDINAL TRIM AND STATIC LATERAL STABILITY CHARACTERISTICS OF THREE FIGHTER-TYPE AIRPLANE MODELS

By Byron M. Jaquet and H. S. Fletcher

Langley Aeronautical Laboratory
Langley Field, Va.

CLASSIFICATION CHANGED
UNCLASSIFIED

NATIONAL ADVISORY COMMITTEE FOR AERONAUTICS

WASHINGTON

September 11, 1956

[redacted]

UNCLASSIFIED

NACA RM L56F19

NATIONAL ADVISORY COMMITTEE FOR AERONAUTICS

RESEARCH MEMORANDUM

WIND-TUNNEL INVESTIGATION AT LOW SPEED OF EFFECTS OF SIDESLIP ON STATIC LONGITUDINAL TRIM AND STATIC LATERAL STABILITY CHARACTERISTICS OF THREE FIGHTER-TYPE AIRPLANE MODELS

By Byron M. Jaquet and H. S. Fletcher

SUMMARY

A wind-tunnel investigation was made at low speed in the Langley stability tunnel to determine the effects of sideslip on the static longitudinal trim characteristics of three fighter-type airplane models. Static lateral stability data for the models are also presented but are not discussed. The models consisted of a 45° swept-wing model with a horizontal tail which was geometrically similar to the wing and was mounted in a position slightly below the wing, a clipped-delta-wing model with a horizontal tail which also was geometrically similar to the wing but was mounted in a moderately high position with respect to the wing, and a 60° delta-wing model which did not have a horizontal tail.

The results of the investigation have indicated that the clipped-delta-wing model had the greatest variation of pitching-moment coefficient with angle of sideslip and this variation occurred throughout the lift-coefficient range and was greatest at high positive lift coefficients. At a lift coefficient of zero, for example, the change in nose-down pitching-moment coefficient in going from an angle of sideslip of 0° to -20° was equivalent to that produced by about 4° incidence of the horizontal tail.

INTRODUCTION

During certain maneuvers, several fighter-type airplanes have encountered uncontrollable motions which resulted in the attainment of large sideslip angles. (See ref. 1, for example.) As a result of these occurrences, knowledge of the effect of sideslip on the static longitudinal stability is of interest. Some information on this subject has been presented in references 2 and 3.

The present low-speed investigation was made as an extension of the work of references 4 and 5 and an unpublished investigation made in the Langley stability tunnel in order to show the effects of sideslip on the static longitudinal trim and static lateral stability characteristics of three fighter-type airplane models for an angle-of-attack range of -28° to 28° and sideslip angles to -30°. The models consisted of a 45° sweptback-wing model (model A), a clipped-delta-wing model (model B), and a 60° delta-wing model (model C). Models A and B had horizontal tails similar in plan form to their wings whereas model C did not have a horizontal tail. Since, for these models, the static longitudinal characteristics were previously investigated only at 0° sideslip and, in general, the static lateral stability characteristics were obtained for sideslip angles of $\pm 5^\circ$ in reference 4 (model A), in reference 5 (model C), and in an unpublished investigation (model B), prime consideration has been given to the longitudinal characteristics of the models. The brief discussion of the lateral characteristics is confined to the linearity of the curves at high angles of attack and sideslip.

SYMBOLS

The data presented herein are referred to the stability system of axes shown in figure 1. The moments were measured about the center-of-gravity positions indicated in figure 2. The symbols and coefficients used herein are defined as follows:

F_L	lift, lb
F_D'	drag, lb
F_Y	side force, lb
M_X	rolling moment, ft-lb
M_Y	pitching moment, ft-lb
M_Z	yawing moment, ft-lb
A	aspect ratio, b^2/S
b	span, ft
S	area, sq ft
c	local chord parallel to plane of symmetry, ft
$\bar{c}$	mean aerodynamic chord, $\frac{2}{S}\int_0^{b/2} c^2 dy$, ft

l	tail length from center of gravity to $\bar{c}/4$ of tail measured parallel to fuselage reference plane, ft
y	spanwise distance measured from and perpendicular to plane of symmetry, ft
z_W	vertical distance of wing above or below fuselage reference line, ft
q	dynamic pressure, $\frac{\rho V^2}{2}$, lb/sq ft
ρ	mass density of air, slugs/cu ft
V	airspeed, ft/sec
α	angle of attack of fuselage reference line, deg
β	angle of sideslip, deg
i_t	horizontal-tail incidence angle, deg
C_L	lift coefficient, $\frac{F_L}{qS_W}$
C_D'	drag coefficient, $\frac{F_D'}{qS_W}$
C_Y	side-force coefficient, $\frac{F_Y}{qS_W}$
C_l	rolling-moment coefficient, $\frac{M_X}{qS_W b_W}$
C_m	pitching-moment coefficient, $\frac{M_Y}{qS_W \bar{c}_W}$
C_n	yawing-moment coefficient, $\frac{M_Z}{qS_W b_W}$

Subscripts:

W	wing
H	horizontal tail
V	vertical tail

Model-Component Designations

For convenience the model configurations are defined by a grouping of the following symbols which denote model components:

F	fuselage
W	wing
V	vertical tail
H	horizontal tail

APPARATUS AND MODELS

The 6- by 6-foot test section (ref. 6) of the Langley stability tunnel was used for the present investigation. The models were mounted on a single support strut which was rigidly attached to a six-component balance system.

A three-view drawing of each of the models is presented in figure 2 and additional model details are presented in table I. Photographs of model B in the 6- by 6-foot test section of the Langley stability tunnel are presented as figure 3. Model A was previously used for the investigation of reference 4 and model C was previously used for the investigation of reference 5. With a few exceptions, the air inlets and exit for model B were open. Models A and C were solid throughout. All models were constructed of laminated mahogany with aluminum-alloy trailing edges on the wings and tails to prevent warpage.

TESTS

The tests consisted of six-component measurements of the aerodynamic forces and moments through an angle-of-attack range of -28° to 28° at sideslip angles of 0°, -6°, -12°, -20°, and -30° for the complete models (complete model C did not have a horizontal tail) and at sideslip angles of 0°, -12°, -20°, and -30° for models A and B with their horizontal tails removed. For complete model A, data were also obtained at $\beta = -25^\circ$ over an angle-of-attack range of $\pm 12^\circ$. Data were obtained at angles of attack of -8°, -12°, and -16° through a sideslip range from 4° up to -30° for each model (horizontal tail on and off for models A and B).

Inasmuch as the effect of sideslip on the longitudinal characteristics of model B was rather large, even at $C_L = 0$, some additional data were obtained on this model. At angle of attack of 0°, data were obtained, over

a sideslip range of 4° to -30°, with the original fuselage, horizontal tail on ($i_t = 0°$) and off, and with the faired fuselage shown in figures 2 and 3, horizontal tail on ($i_t = 0°, -4°$) and off. Data were also obtained over the same sideslip range for complete model B with the faired fuselage and with the leading-edge slats fully extended. With ($i_t = 0°$) and without the horizontal tail, model B was also tested with the faired fuselage over an angle-of-attack range of ±12° at $\beta = 0°$ and -6°. The wing alone was mounted in a low position with respect to the model center of gravity and was tested through the sideslip range at $\alpha = 0°$. In mounting the wing for these tests, relatively thick brackets were required and, consequently, the drag coefficients presented herein are probably not truly representative of the drag of the wing alone; this is especially true at large sideslip angles where the drag of the brackets approaches that of a flat plate normal to the wind.

All tests were made at a dynamic pressure of 24.9 lb/sq ft and a Mach number of 0.13. The test Reynolds numbers were 0.876×10^6, 1.013×10^6, and 1.650×10^6 based on the mean aerodynamic chord of models A, B, and C, respectively.

CORRECTIONS

Approximate jet boundary corrections (ref. 7) were applied to the angle of attack and drag coefficient. Horizontal tail-on pitching-moment coefficients were corrected for the effects of the jet boundaries by the methods of reference 8. The data were not corrected for the effects of the support strut or blockage; on the basis of past experience, they would be negligible.

RESULTS AND DISCUSSION

Presentation of Results

Aerodynamic characteristics are shown by the variation of the coefficients C_L, C_D', C_m, C_Y, C_n, and C_l with angle of attack for several angles of sideslip presented in figures 4, 5, and 6 for models A, B, and C, respectively. In figure 7 is presented, for each model, the variation of C_m with C_L, for several angles of sideslip and in figure 8 is presented, for several lift coefficients, the variation of C_m with β for models A and B with their horizontal tails on ($i_t = 0°$) and off and for complete model C which did not have a horizontal tail. The variation of the coefficients with angle of sideslip for angles of attack of about -8°,

-12°, and -16° is presented in figures 9, 10, and 11 for each model. (These data are in agreement with those obtained through the angle-of-attack range at a constant sideslip angle.) In figure 12 is shown the variation of the coefficients at $\alpha = 0^\circ$ for model B with ($i_t = 0^\circ$) and without the horizontal tail and for the wing alone of model B. The effect, for model B, of fuselage fairing, leading-edge slat deflection, and horizontal-tail incidence on the variation, at $\alpha = 0^\circ$, of the coefficients with angle of sideslip is presented in figure 13.

Static Longitudinal Stability

Briefly, in regard to the basic data of figures 4 to 6, the lift coefficient for all models decreases with an increase in the angle of sideslip. Model C, which is more symmetrical with respect to the fuselage reference plane, has lift and pitching-moment curves that are almost antisymmetrical at corresponding positive and negative angles of attack. The lack of antisymmetry in these curves for models A and B is the result of the relative position of the wing and horizontal tail on the fuselage. Information on the effects of the wing and the horizontal-tail position on the static longitudinal stability is presented in references 2 and 9.

The static longitudinal stability of the models is generally affected by changes in sideslip angle only at high lift coefficients and at large sideslip angles (figs. 7(a), 7(b), and 7(c)). The pitch-up tendency that occurs for complete model A at about $C_L = 0.56$ ($\beta = 0^\circ$) is relatively unaffected by changes in sideslip angle up to about -20°; at larger angles of sideslip, it appears that the model may have greater stability in this lift-coefficient region although the data are rather sparse for a definite conclusion. At about a corresponding negative lift coefficient, the pitch-down tendency at $\beta = 0^\circ$ is reduced only slightly by a change in the angle of sideslip. Pitch-up also occurs for complete model B (fig. 7(b)) but at a higher lift coefficient (about $C_L = 0.75$) than that occurring for model A. This pitch-up is relatively unaffected by changes in the angle of sideslip and there is no tendency for pitch-up in the negative lift-coefficient range. At $\beta = 0^\circ$ there are no tendencies for pitch-up or pitch-down for model C but when $\beta \approx -30^\circ$ is reached these tendencies do appear at lift coefficients of about 0.65 and -0.48. In general, regardless of the sideslip angle, the largest variation of static longitudinal stability with lift coefficient occurs for model A, whereas the least variation occurs for model C.

Variation of Pitching-Moment Coefficient With Sideslip

Of the three models investigated, the greatest variation of pitching-moment coefficient with angle of sideslip occurs for model B (figs. 7(b) and 8(b)) and this variation occurs throughout the lift-coefficient range

and is greatest at high positive lift coefficients. Model C, in general, has the least variation of pitching-moment coefficient with angle of sideslip.

On the basis of the horizontal-tail effectiveness determined from the data of figure 13(a), the change in nose-down pitching-moment coefficient at $C_L = 0$ (fig. 7(b)) resulting from a change in the angle of sideslip from 0° to about -20° is equivalent to that produced by a deflection of the horizontal tail of about 4°.

The effect of sideslip on the contribution of the horizontal tail to the pitching-moment coefficient is largest for model B (compare fig. 8(a) with fig. 8(b)) and this fact and the fact that there is generally little effect of sideslip on the wing-fuselage contribution to the pitching-moment coefficient (figs. 8 and 12) probably accounts for the large variation of pitching-moment coefficient with angle of sideslip for model B. The pitching-moment coefficient of the wing alone of model B at $\alpha = 0^\circ$ (fig. 12) is relatively unaffected by changes in the angle of sideslip.

The foregoing results are, in general, similar to those presented in reference 2 in that the low-aspect-ratio delta-wing model (model C) experienced the least effect of sideslip on the pitching-moment characteristics.

Effect of Modifications to Model B on Static Longitudinal Stability and Variation of Pitching-Moment Coefficient With Sideslip

Since complete model B experienced a large effect of sideslip on the pitching-moment coefficient, some additional data were obtained with the fuselage faired as shown in figures 2 and 3 in order to determine the influence of eliminating the rather large ducts. There is, in general, only a small effect of eliminating the ducts (by fairing the fuselage) on the variation of C_m with C_L for model B with or without the horizontal tail (fig. 7(d)) and there was little effect on the variation of the pitching-moment coefficient with angle of sideslip at $\alpha = 0^\circ$ (fig. 13(a)).

Some additional data were obtained with the faired fuselage model with the leading-edge slats extended and with the horizontal tail at an angle of incidence of -4°. These data (fig. 13(a)) indicate that a negative increment in C_m is produced by extending the slats and that the increment was about constant for the sideslip range investigated. An angle of incidence of the horizontal tail of -4° produced a large positive increment in the pitching-moment coefficient, as would be expected, and this increment also was about constant for sideslip angles less than -24°.

Static Lateral Stability

Only brief consideration will be given to the static lateral data of the models since there was some overlapping of the range of test variables of the present investigation and those of reference 4 (model A), reference 5 (model C), and an unpublished investigation of model B. The lateral data for the large angle-of-attack and sideslip ranges may be of some use in analog-computer studies of combined lateral and longitudinal motions.

At high angles of attack, all models exhibited nonlinearities in the variation of the rolling- and yawing-moment coefficients with angle of sideslip (figs. 4 to 6 and figs. 9 to 11). Also, the rolling- and yawing-moment coefficients of models A and B were appreciably affected by their horizontal tails (figs. 4(e), 4(f), 5(e), and 5(f)). All models became directionally unstable at certain angles of attack and sideslip. This instability occurred in some cases at an angle of attack of 0° (figs. 4, 5, and 12) for large sideslip angles.

CONCLUSIONS

Results of a wind-tunnel investigation at low speed, made to determine the effects of sideslip on the static longitudinal trim characteristics of three fighter-type airplane models, have indicated the following conclusions:

1. Of the three models investigated, a clipped-delta-wing model, having a horizontal tail in a moderately high position relative to the wing, had the greatest variation of pitching-moment coefficient with angle of sideslip and this variation occurred throughout the lift-coefficient range and was greatest at high positive lift coefficients. For example, at a lift coefficient of zero, the nose-down pitching-moment coefficient produced in going from an angle of sideslip of 0° to -20° was equivalent to that produced by about 4° incidence of the horizontal tail.

2. A 60° delta-wing model without a horizontal tail had the least variation of pitching-moment coefficient and static longitudinal stability with angle of sideslip.

3. For all angles of sideslip investigated, a 45° swept-wing model, having a horizontal tail slightly below the wing, had the greatest variation of stability with lift coefficient for the moderate positive and negative lift-coefficient range.

Langley Aeronautical Laboratory,
National Advisory Committee for Aeronautics,
Langley Field, Va., June 1, 1956.

REFERENCES

1. NACA High-Speed Flight Station: Flight Experience With Two High-Speed Airplanes Having Violent Lateral-Longitudinal Coupling in Aileron Rolls. NACA RM H55A13, 1955.

2. Polhamus, Edward C.: Some Factors Affecting the Variation of Pitching Moment With Sideslip of Aircraft Configurations. NACA RM L55E20b, 1955.

3. Goodson, Kenneth W.: Some Effects of Ailerons on the Variation of Aerodynamic Characteristics With Sideslip at Low Speed. NACA RM L55L20, 1956.

4. Jaquet, Bryon M., and Fletcher, H. S.: Wind-Tunnel Investigation at Low Speed of Sideslipping, Rolling, Yawing, and Pitching Characteristics for a Model of a 45° Swept-Wing Fighter-Type Airplane. NACA RM L55F21, 1955.

5. Goodman, Alex, and Thomas, David F., Jr.: Effects of Wing Position and Fuselage Size on the Low-Speed Static and Rolling Stability Characteristics of a Delta-Wing Model. NACA Rep. 1224, 1955. (Supersedes NACA TN 3063.)

6. Bird, John D., Jaquet, Byron M., and Cowan, John W.: Effect of Fuselage and Tail Surfaces on Low-Speed Yawing Characteristics of a Swept-Wing Model As Determined in Curved-Flow Test Section of the Langley Stability Tunnel. NACA TN 2483, 1951. (Supersedes NACA RM L8G13.)

7. Silverstein, Abe, and White, James A.: Wind-Tunnel Interference With Particular Reference to Off-Center Positions of the Wing and to the Downwash at the Tail. NACA Rep. 547, 1936.

8. Gillis, Clarence L., Polhamus, Edward C., and Gray, Joseph L., Jr.: Charts for Determining Jet-Boundary Corrections for Complete Models in 7- by 10-Foot Closed Rectangular Wind Tunnels. NACA WR L-123, 1945. (Formerly NACA ARR L5G31.)

9. Goodman, Alex: Effects of Wing Position and Horizontal-Tail Position on the Static Stability Characteristics of Models With Unswept and 45° Sweptback Surfaces With Some Reference to Mutual Interference. NACA TN 2504, 1951.

TABLE I

GEOMETRIC CHARACTERISTICS OF MODELS

	Model A	Model B	Model C
Wing:			
Aspect ratio	3.56	2.91	2.31
Taper ratio	0.30	0.226	0
Span, ft	3.018	2.750	3.042
Area, sq ft	2.567	2.600	4.005
Root chord, ft	1.309	1.550	2.635
Mean aerodynamic chord, ft	0.935	1.080	1.758
Quarter-chord sweep angle, deg	45	33.21	52.2
Dihedral angle, deg	0	2.67	0
Geometric twist, deg	0	0	0
Incidence, deg	0	0	0
NACA airfoil section parallel to plane of symmetry:			
Root	$64_{(06)}$A007	0008(modified)	65A003
Tip		0005(modified)	65A003
Wing-height ratio, Z_W/b_W	-0.0525	-0.0691	0
Slat rotation about hinge line for fully opened position, deg		24	
Horizontal tail:			None used
Aspect ratio	3.56	2.80	
Taper ratio	0.30	0.225	
Span, ft	1.548	1.133	
Area, sq ft	0.676	0.459	
Root chord, ft	0.670	0.667	
Mean aerodynamic chord, ft	0.479	0.466	
Quarter-chord sweep angle, deg	45	34.37	
Dihedral angle, deg	0	0	
Geometric twist, deg	0	0	
Incidence, deg	0	0,-4	
NACA airfoil section parallel to plane of symmetry:			
Root	64A003.5	0007(modified)	
Tip	64A003.5	0004(modified)	
Tail length from center of gravity to $\bar{c}/4$ of tail, ft	1.148	1.607	
Area ratio, S_H/S_W	0.263	0.177	
Tail volume, $\frac{l_H}{\bar{c}_W}\frac{S_H}{S_W}$	0.323	0.263	
Vertical tail (to reference line):			
Aspect ratio	1.58	1.30	2.18
Taper ratio	0.270	0.167	0
Span, ft	0.797	0.950	1.123
Area, sq ft	0.403	0.692	0.579
Root chord, ft	0.796	1.249	1.029
Mean aerodynamic chord, ft	0.561	0.851	0.687
Quarter-chord sweep angle, deg	45	42	34.5
NACA airfoil section parallel to root chord:			
Root	3.5-percent-thick modified flat plate	0007(modified)	65006
Tip		0004(modified)	65006
Tail length from center of gravity to $\bar{c}/4$ of tail, ft	1.203	1.332	1.738
Area ratio, S_V/S_W	0.157	0.266	0.144
Tail volume, $\frac{l_V}{b_W}\frac{S_V}{S_W}$	0.063	0.129	0.082
Fuselage:			
Length, ft	3.740	3.703	2.700
Fineness ratio	8.03	7.16	9.00

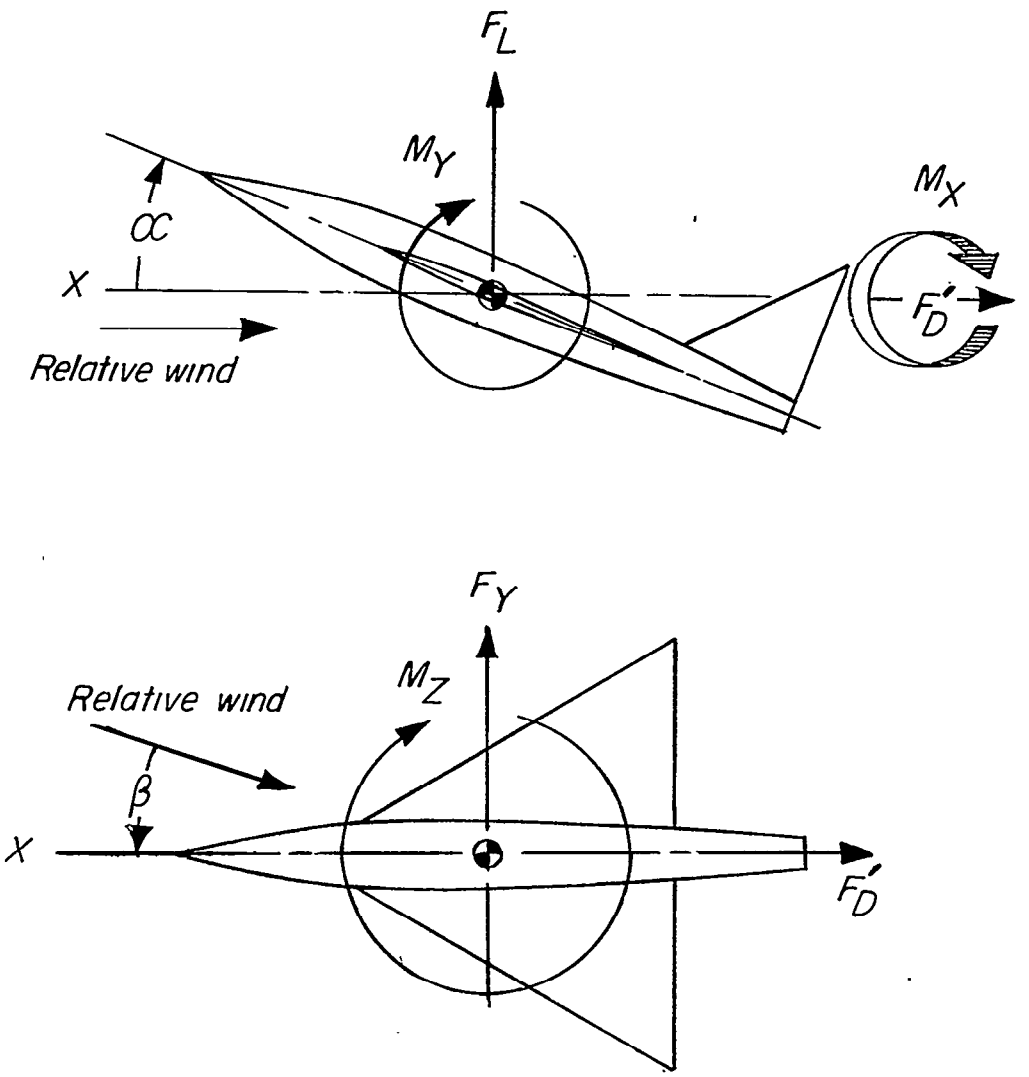

Figure 1.- Stability system of axes. Arrows indicate positive forces, moments, and angular displacements.

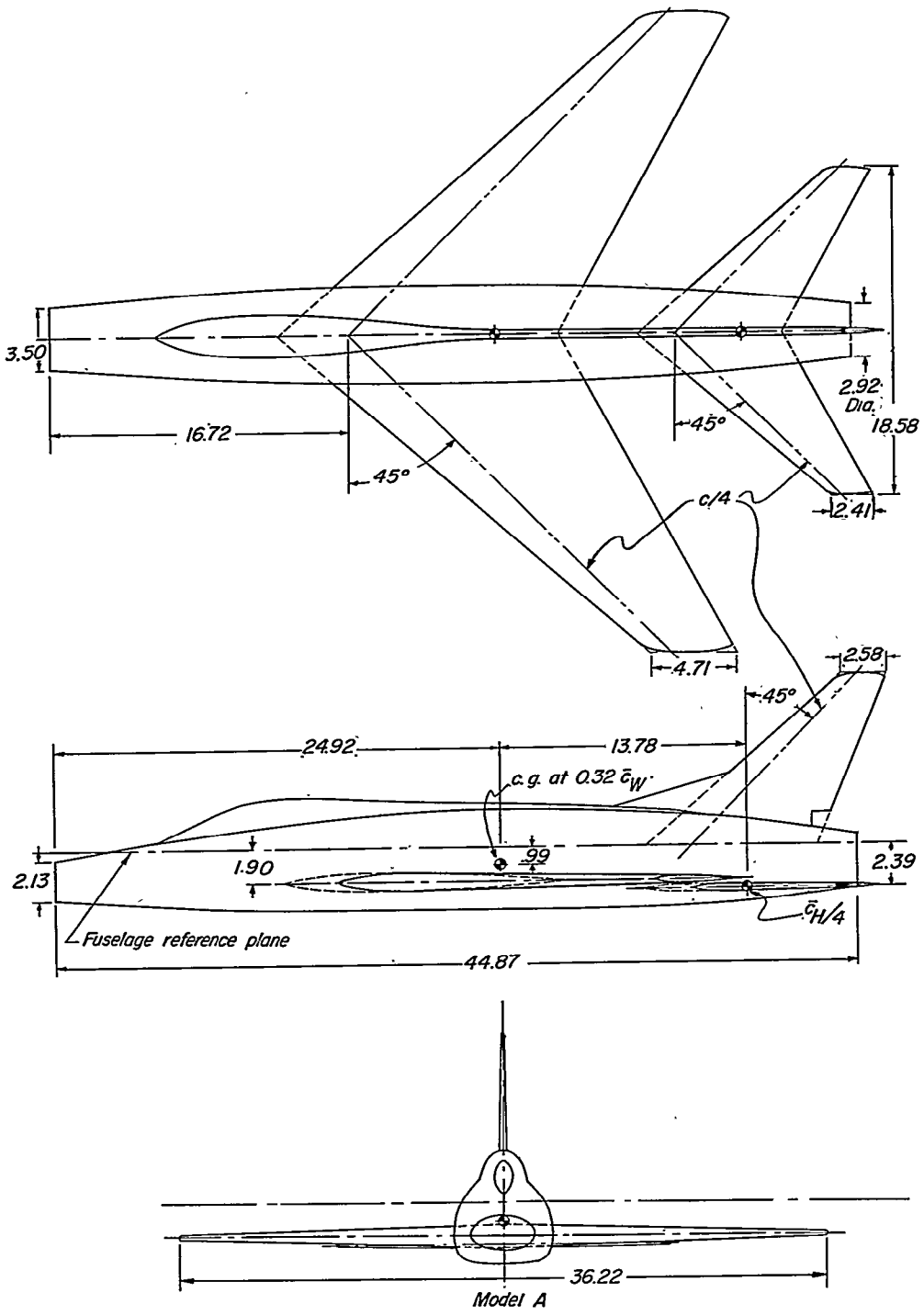

Figure 2.- Geometry of models. Dimensions are in inches.

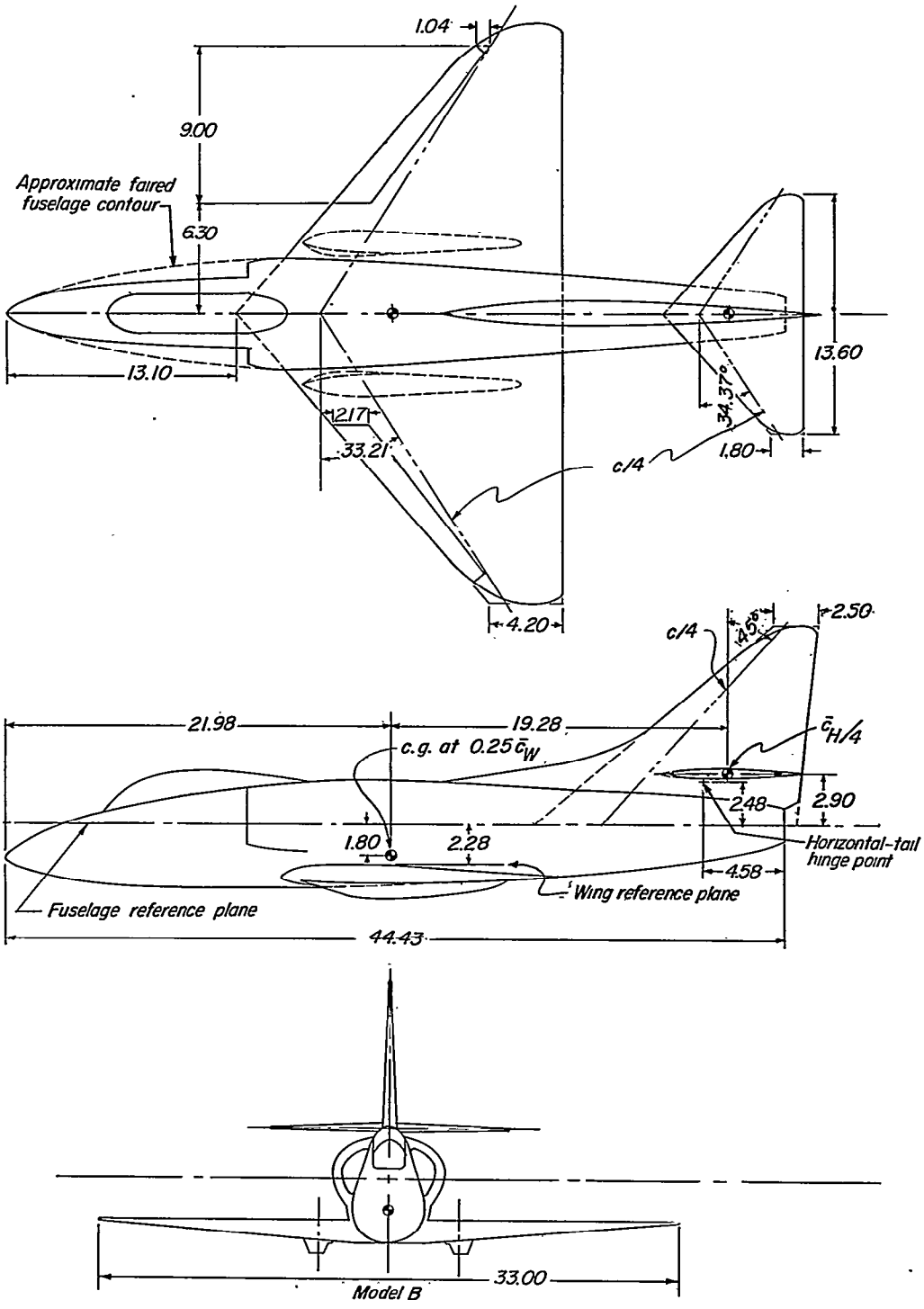

Figure 2.- Continued.

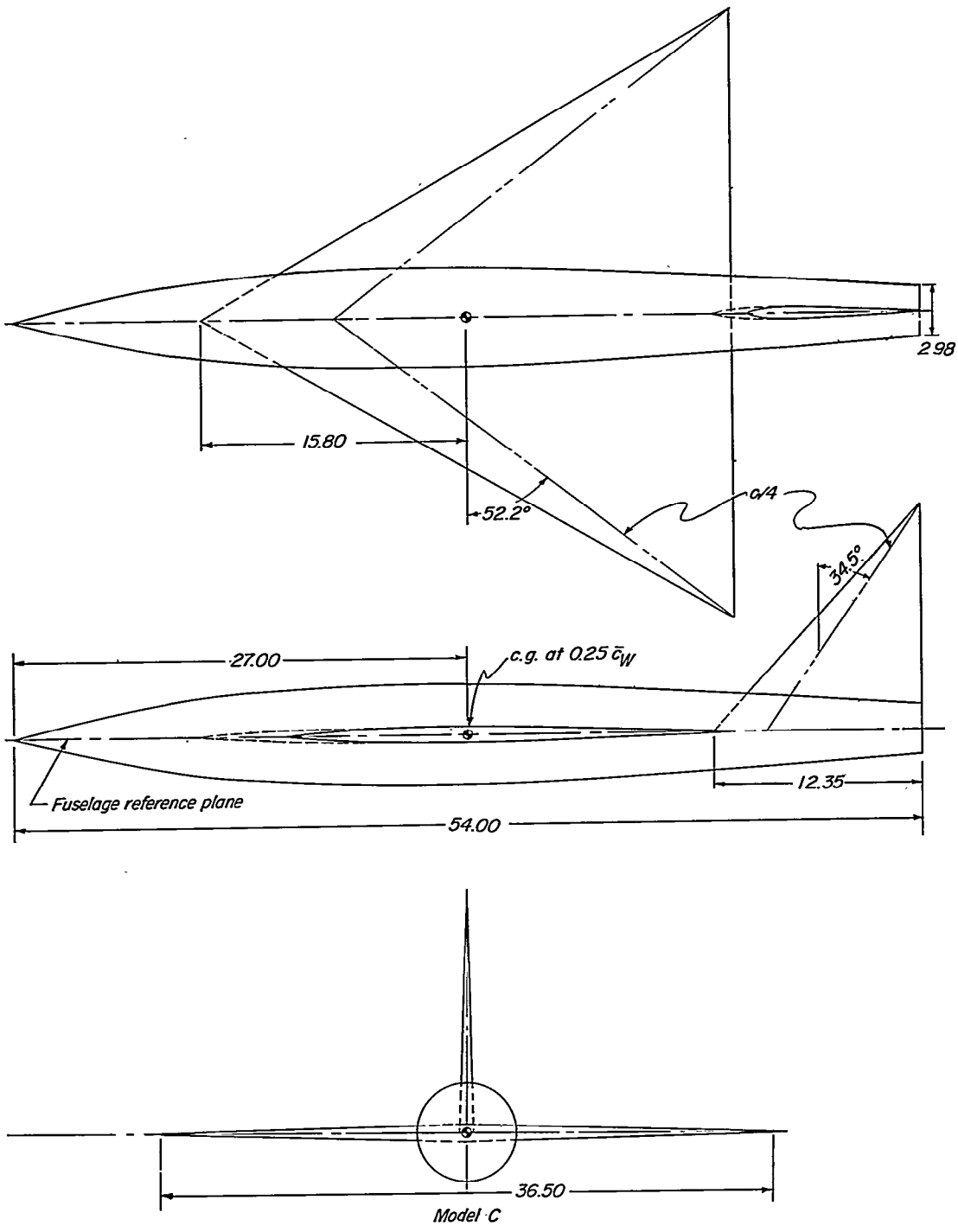

Figure 2.- Concluded.

(a) Original fuselage.

(b) Faired fuselage.

L-93530

Figure 3.- Photographs of model B.

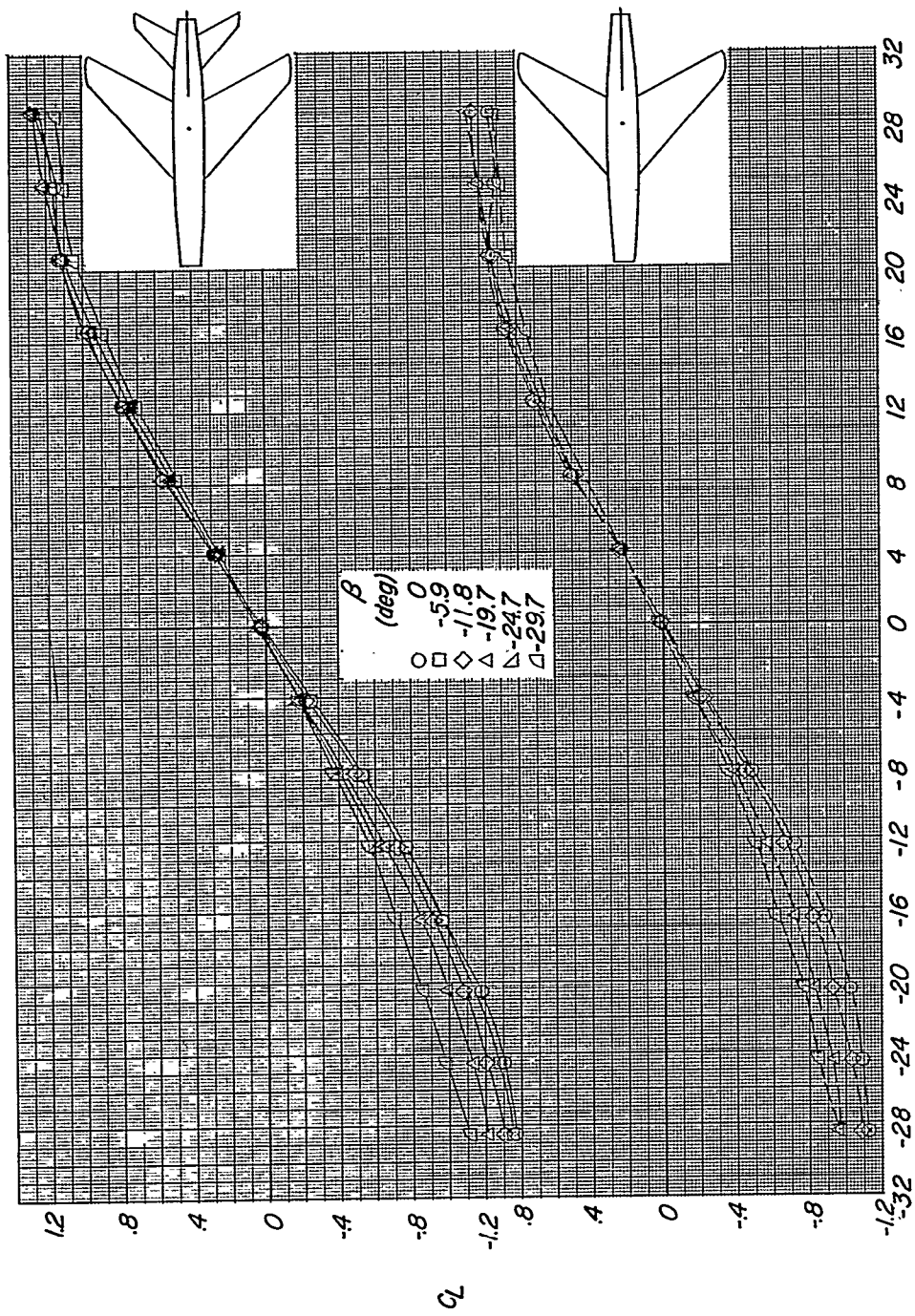

(a) C_L plotted against α. Horizontal tail on $\left(i_t = 0^\circ\right)$ and off.

Figure 4.- Variation of aerodynamic characteristics of model A with angle of attack for several angles of sideslip.

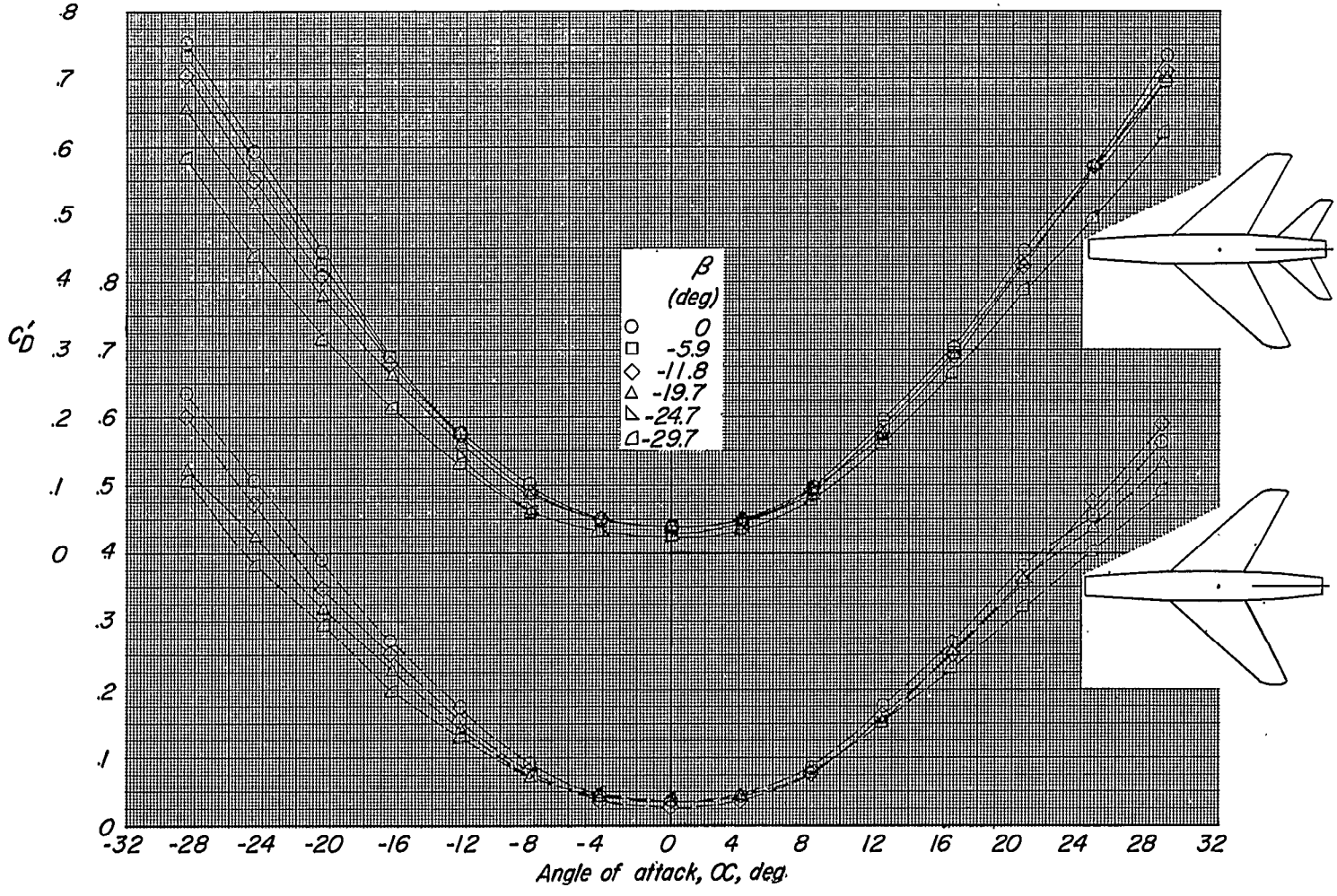

(b) C_D' plotted against α. Horizontal tail on $(i_t = 0^\circ)$ and off.

Figure 4.- Continued.

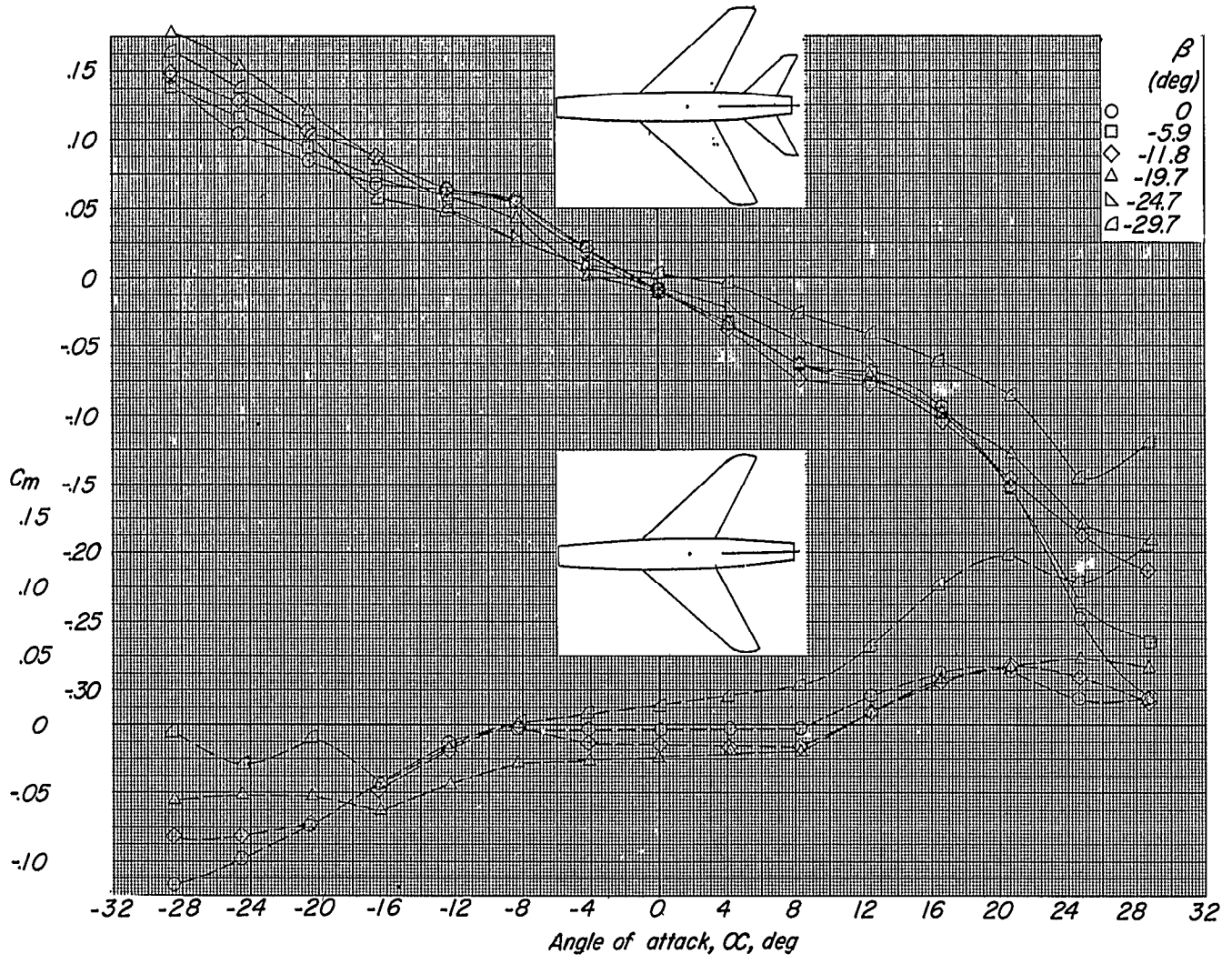

(c) C_m plotted against α. Horizontal tail on $(i_t = 0^\circ)$ and off.

Figure 4.- Continued.

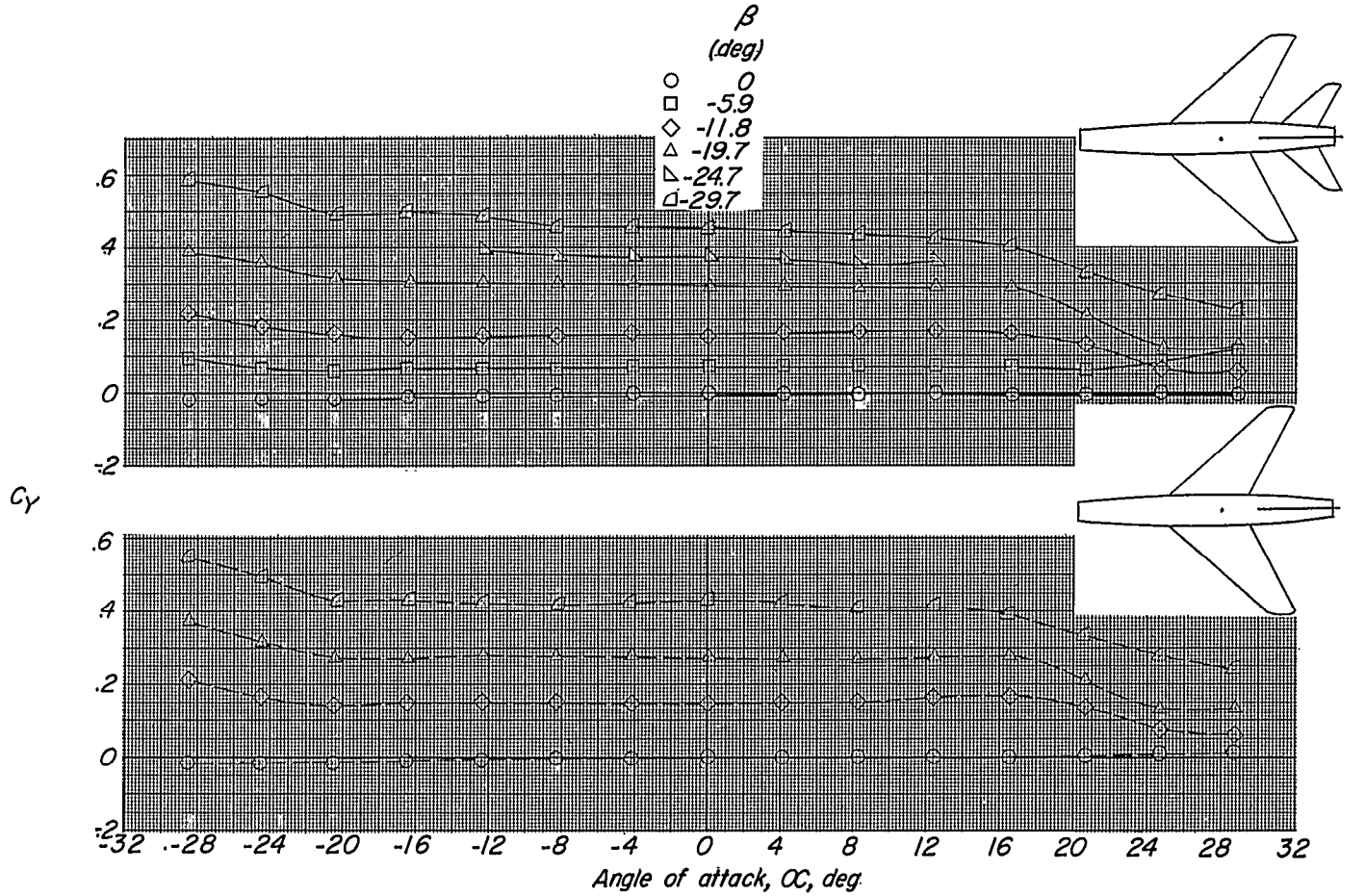

(d) C_Y plotted against α. Horizontal tail on $(i_t = 0^\circ)$ and off.

Figure 4.- Continued.

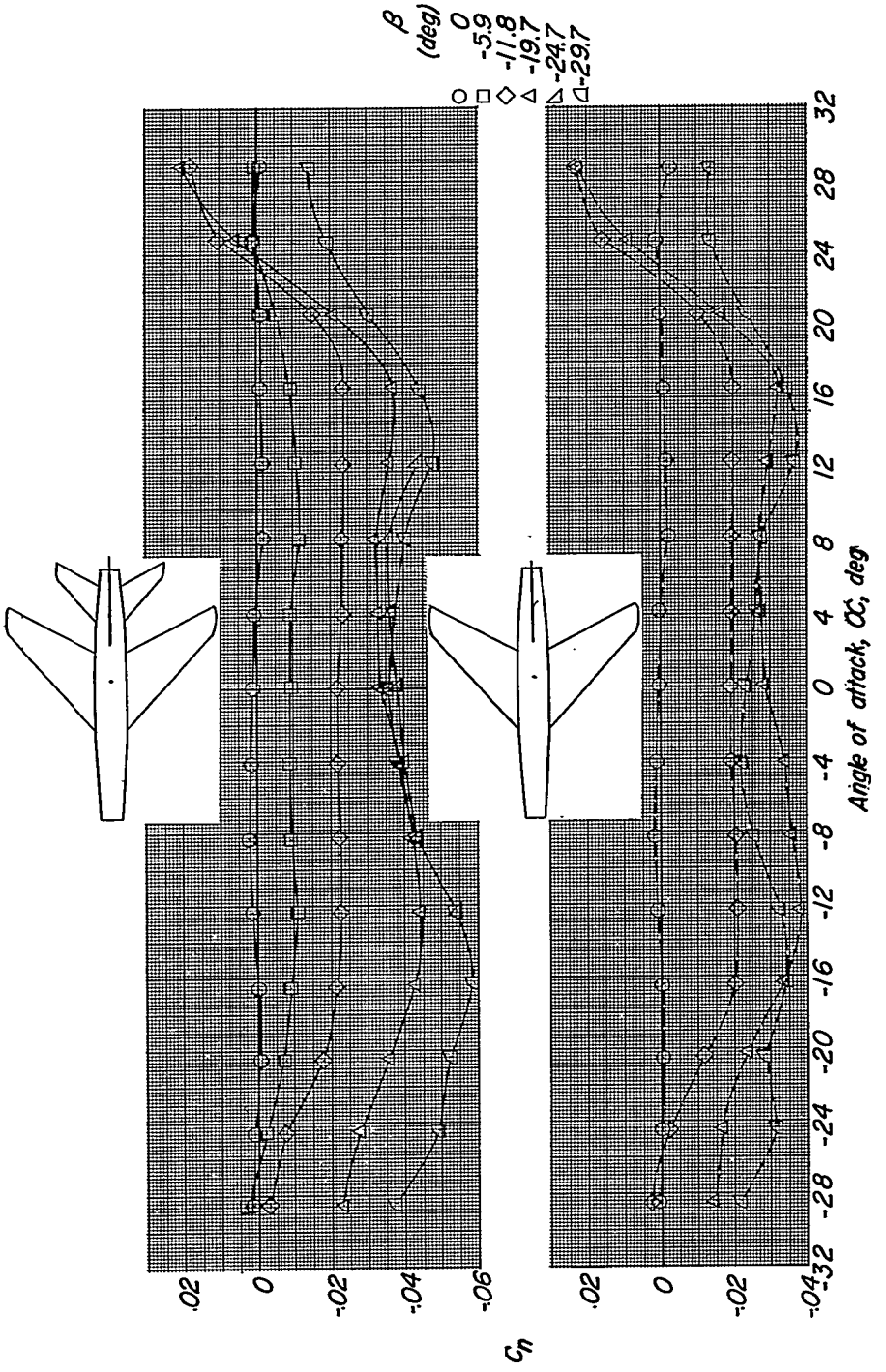

(e) C_n plotted against α. Horizontal tail on $\left(i_t = 0^\circ\right)$ and off.

Figure 4.- Continued.

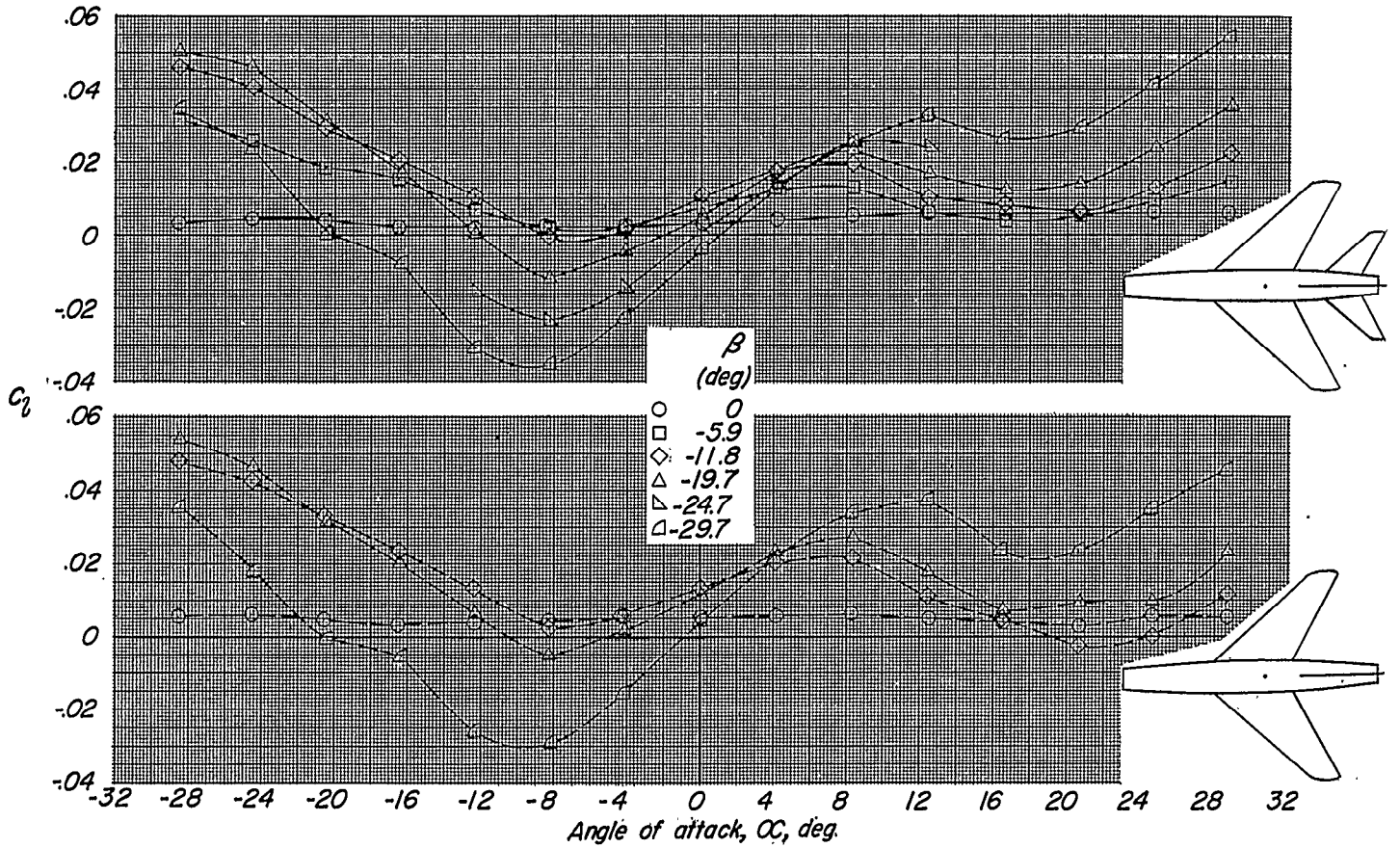

(f) C_l plotted against α. Horizontal tail on $(i_t = 0^\circ)$ and off.

Figure 4.- Concluded.

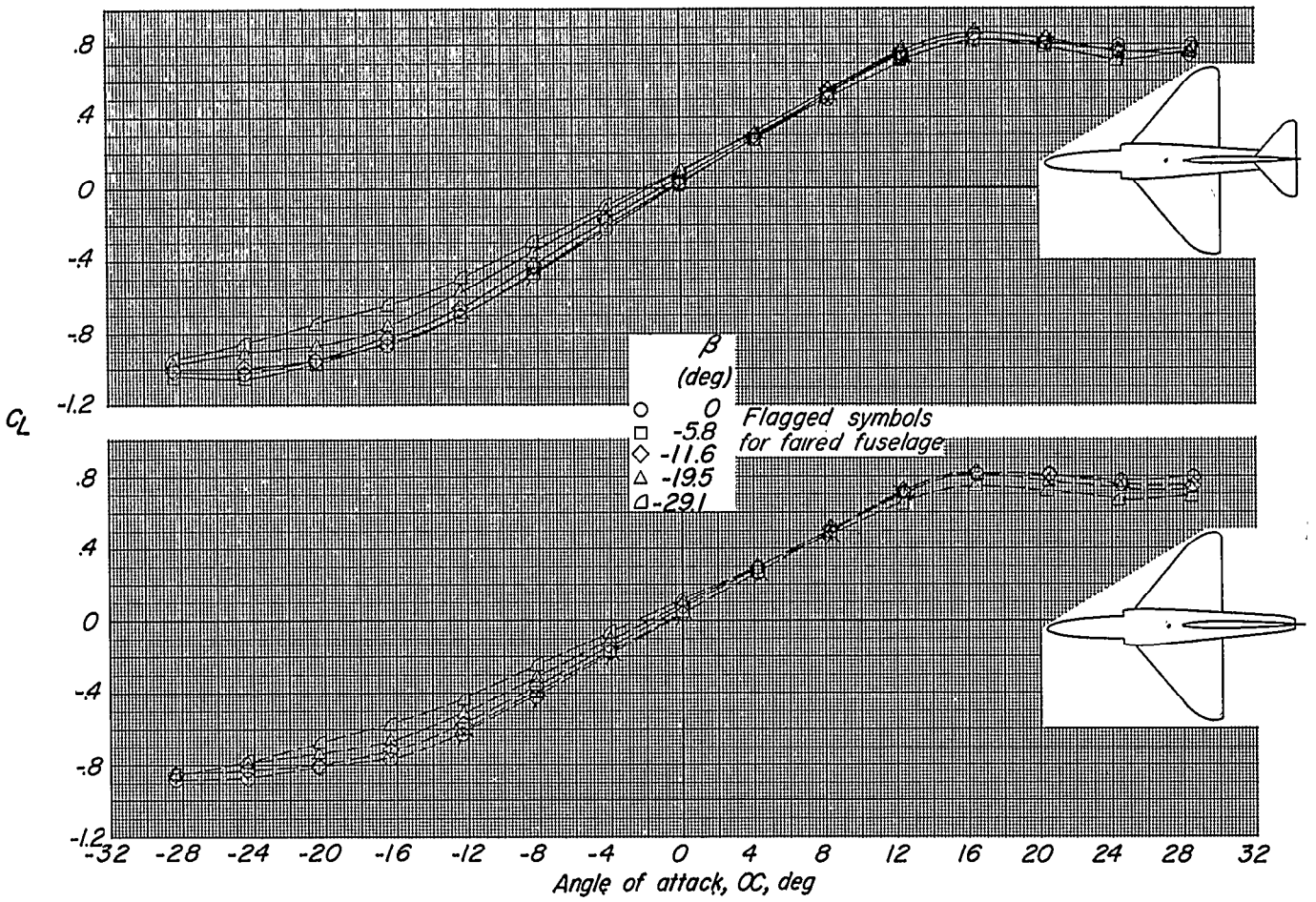

(a) C_L plotted against α. Horizontal tail on $(i_t = 0°)$ and off.

Figure 5.- Variation of aerodynamic characteristics of model B with angle of attack for several angles of sideslip.

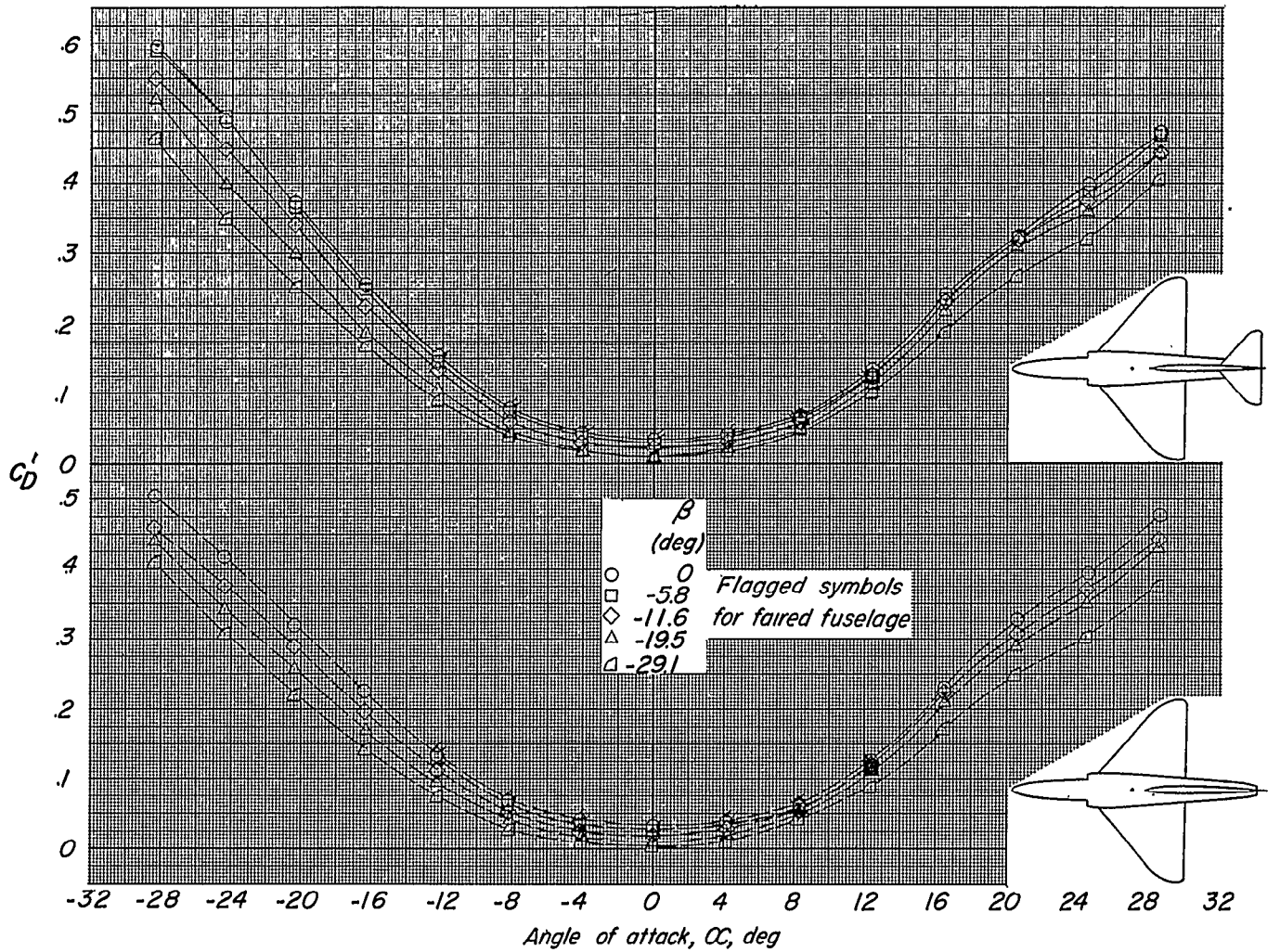

(b) C_D' plotted against α. Horizontal tail on $(i_t = 0^\circ)$ and off.

Figure 5.- Continued.

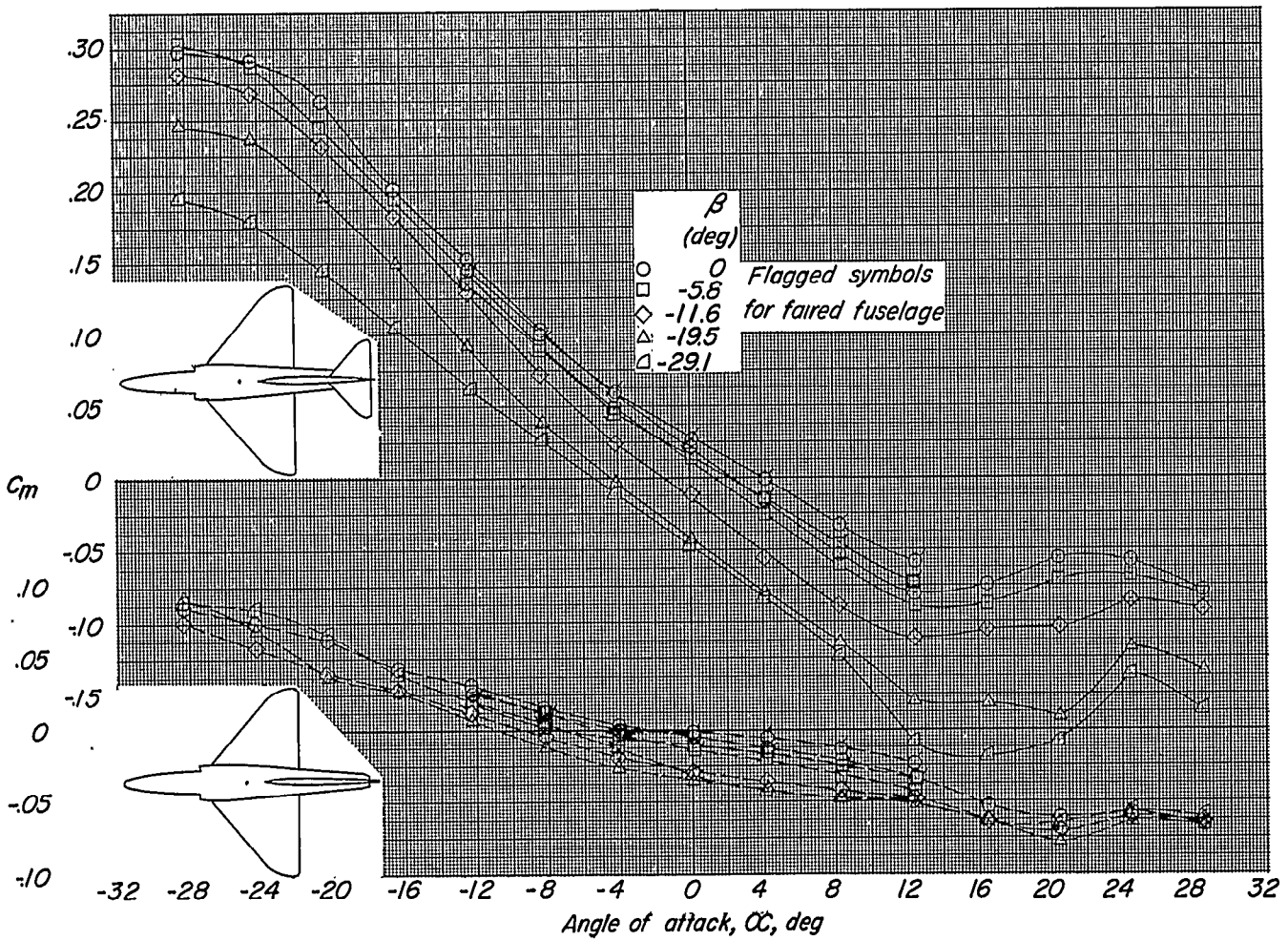

(c) C_m plotted against α. Horizontal tail on $(i_t = 0^\circ)$ and off.

Figure 5.- Continued.

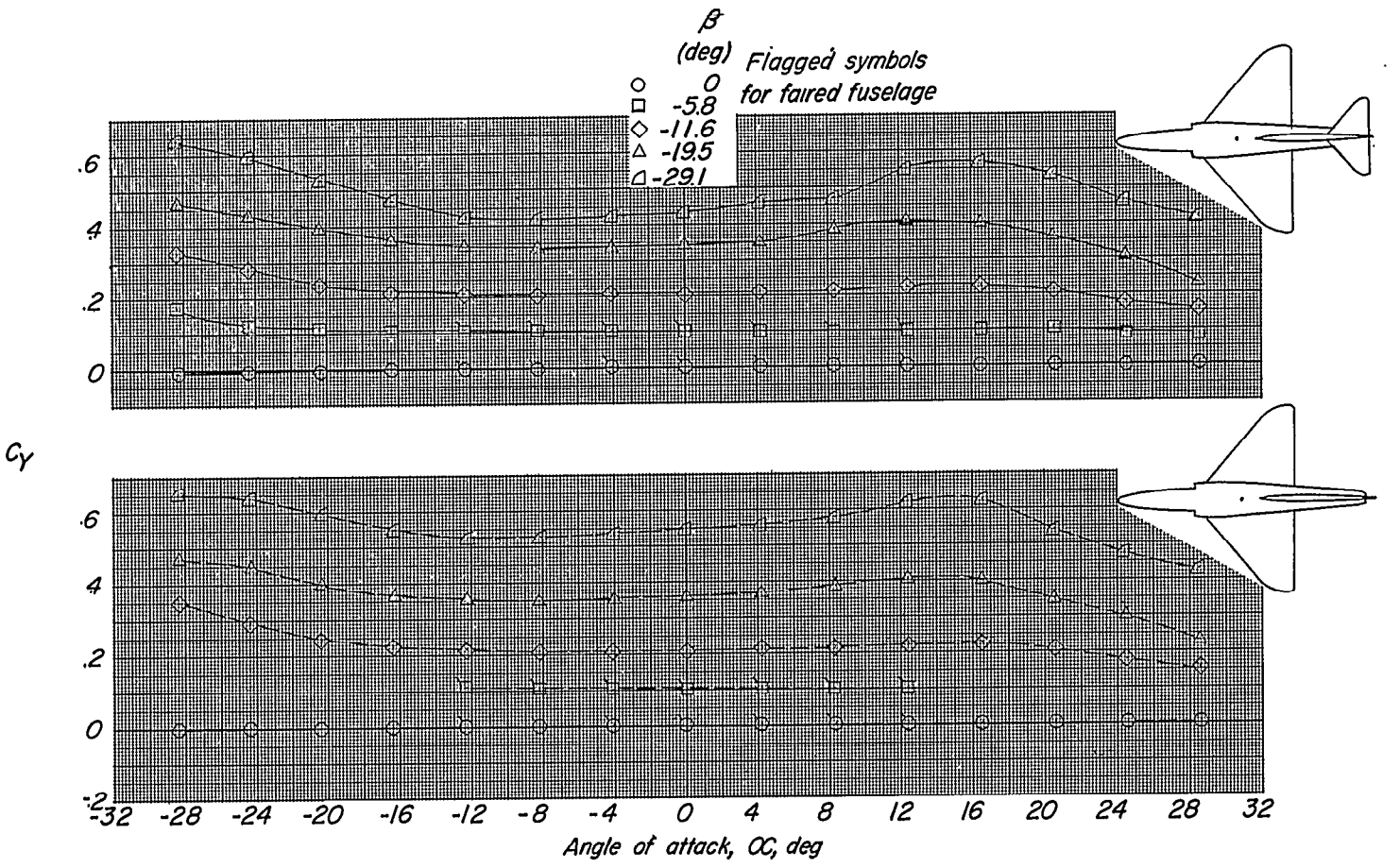

(d) C_Y plotted against α. Horizontal tail on $(i_t = 0^\circ)$ and off.

Figure 5.- Continued.

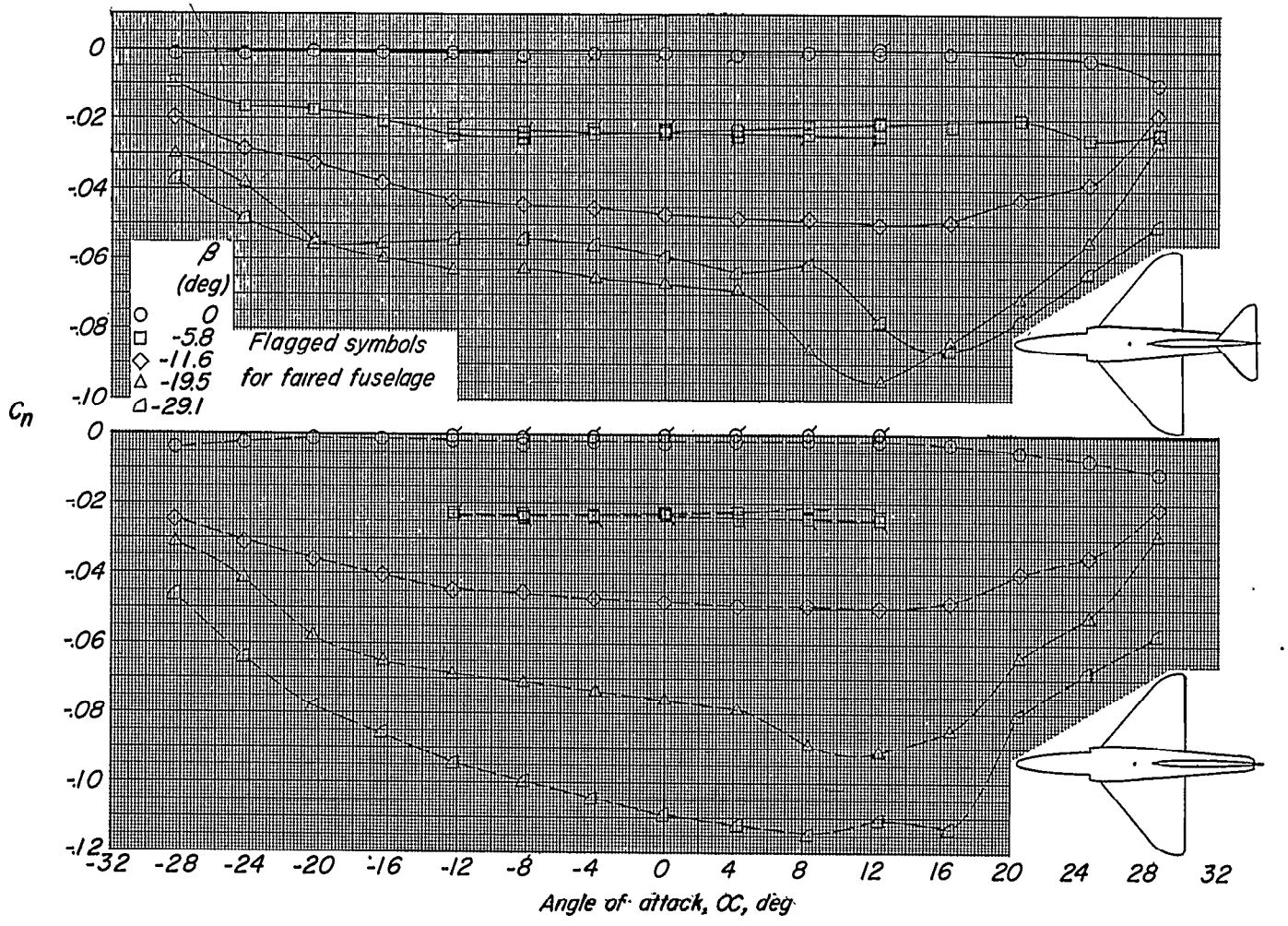

(e) C_n plotted against α. Horizontal tail on $(i_t = 0^\circ)$ and off.

Figure 5.- Continued.

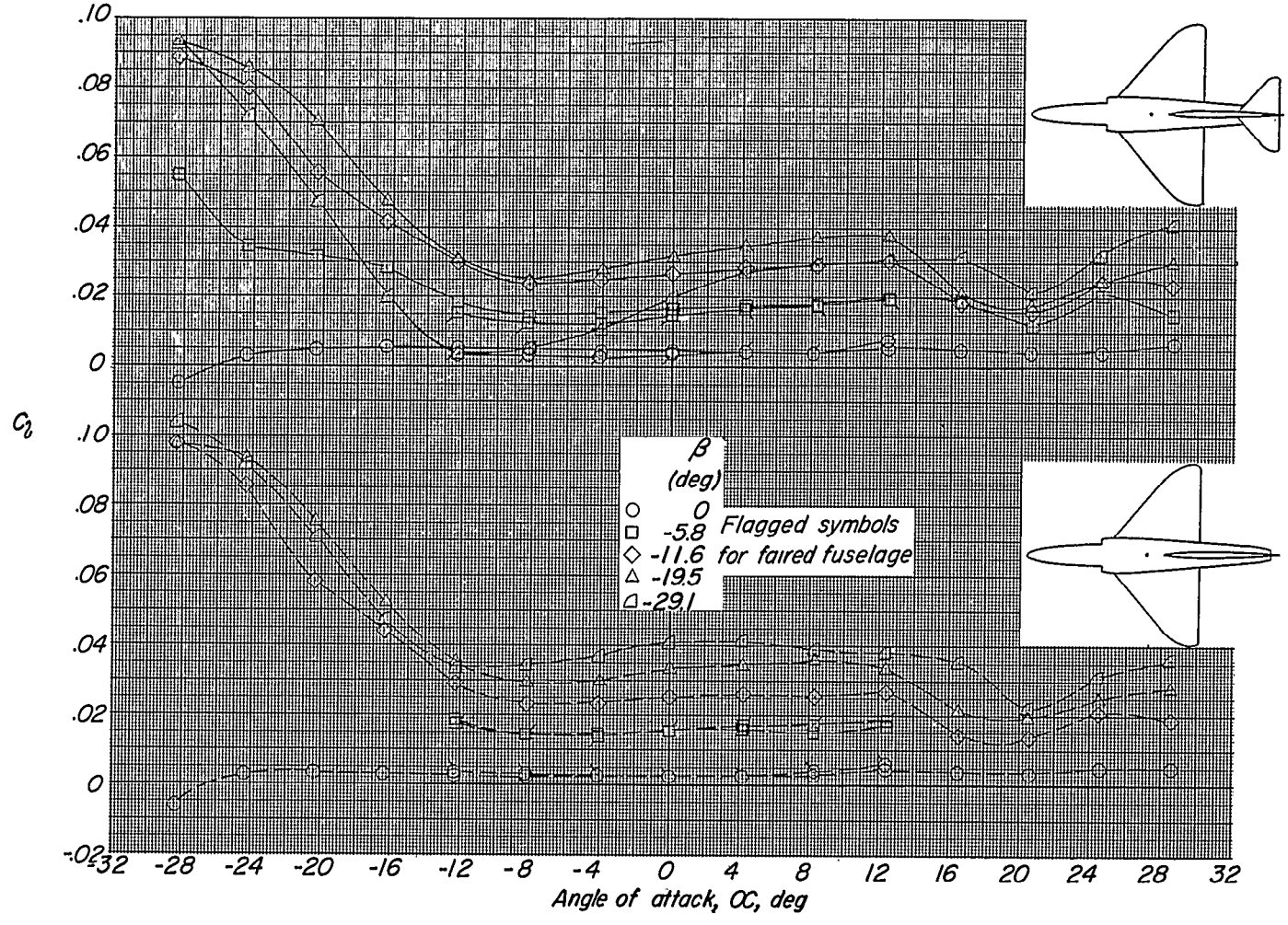

(f) C_l plotted against α. Horizontal tail on $(i_t = 0^o)$ and off.

Figure 5.- Concluded.

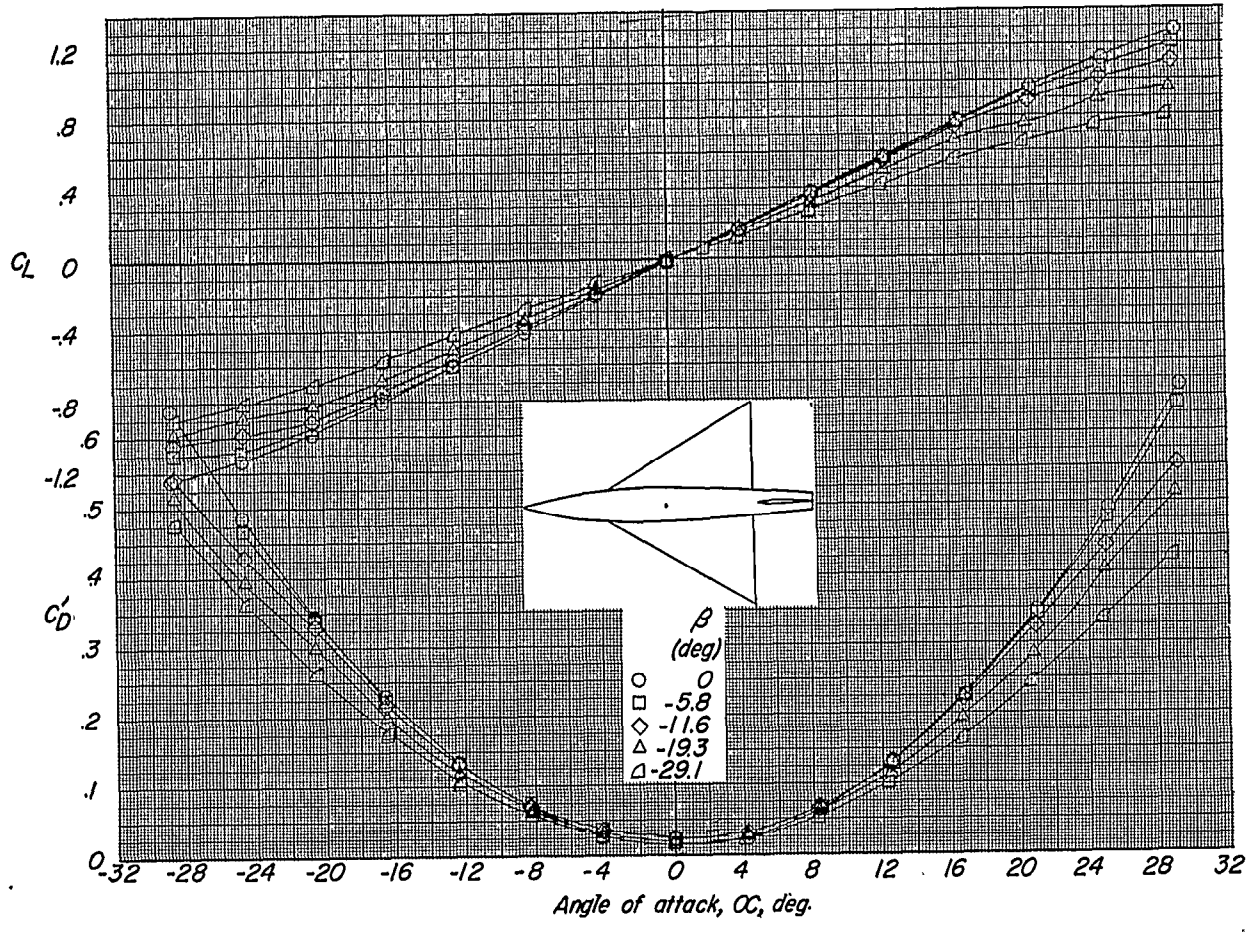

(a) C_L and C_D' plotted against α.

Figure 6.- Variation of aerodynamic characteristics of model C with angle of attack for several angles of sideslip.

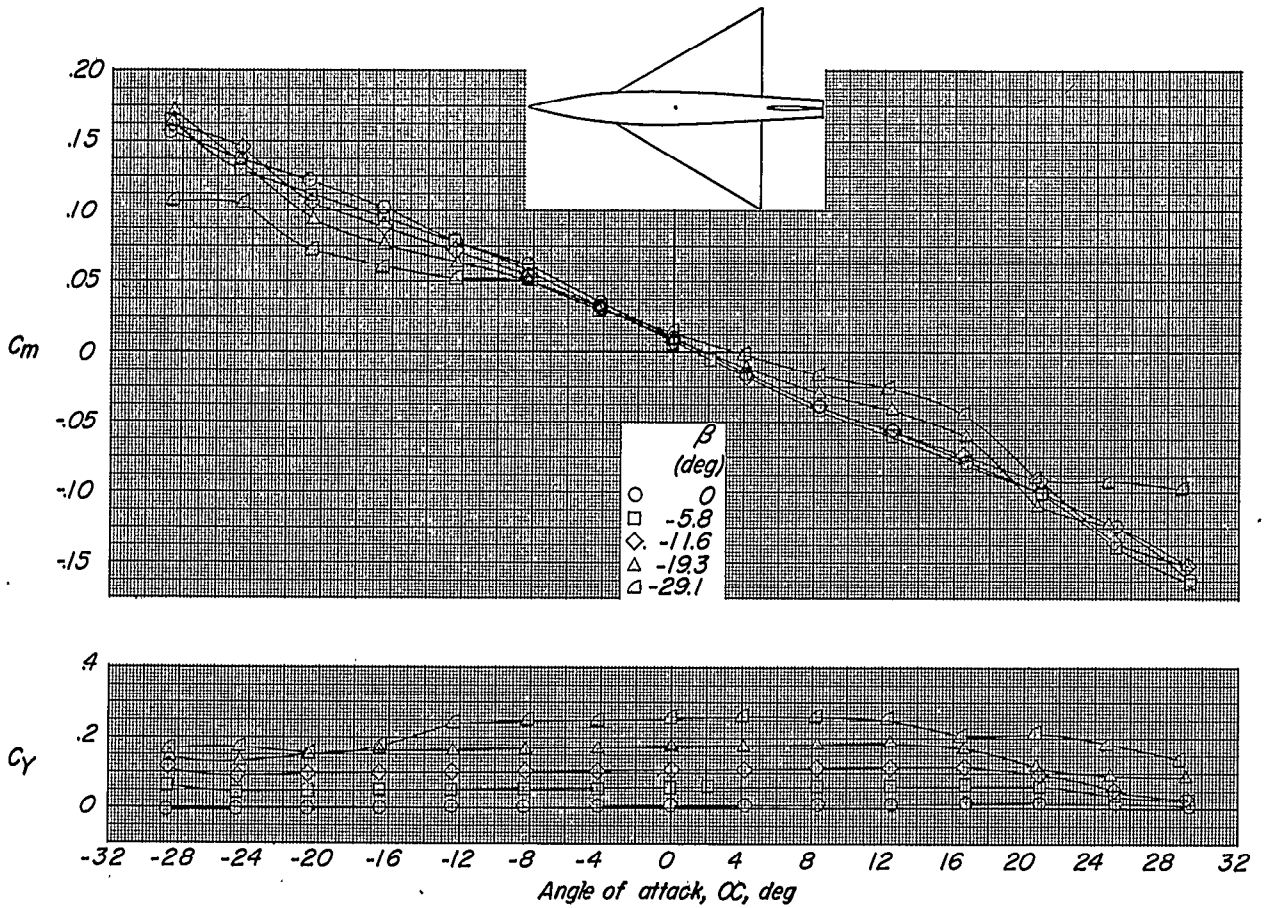

(b) C_m and C_Y plotted against α.

Figure 6.- Continued.

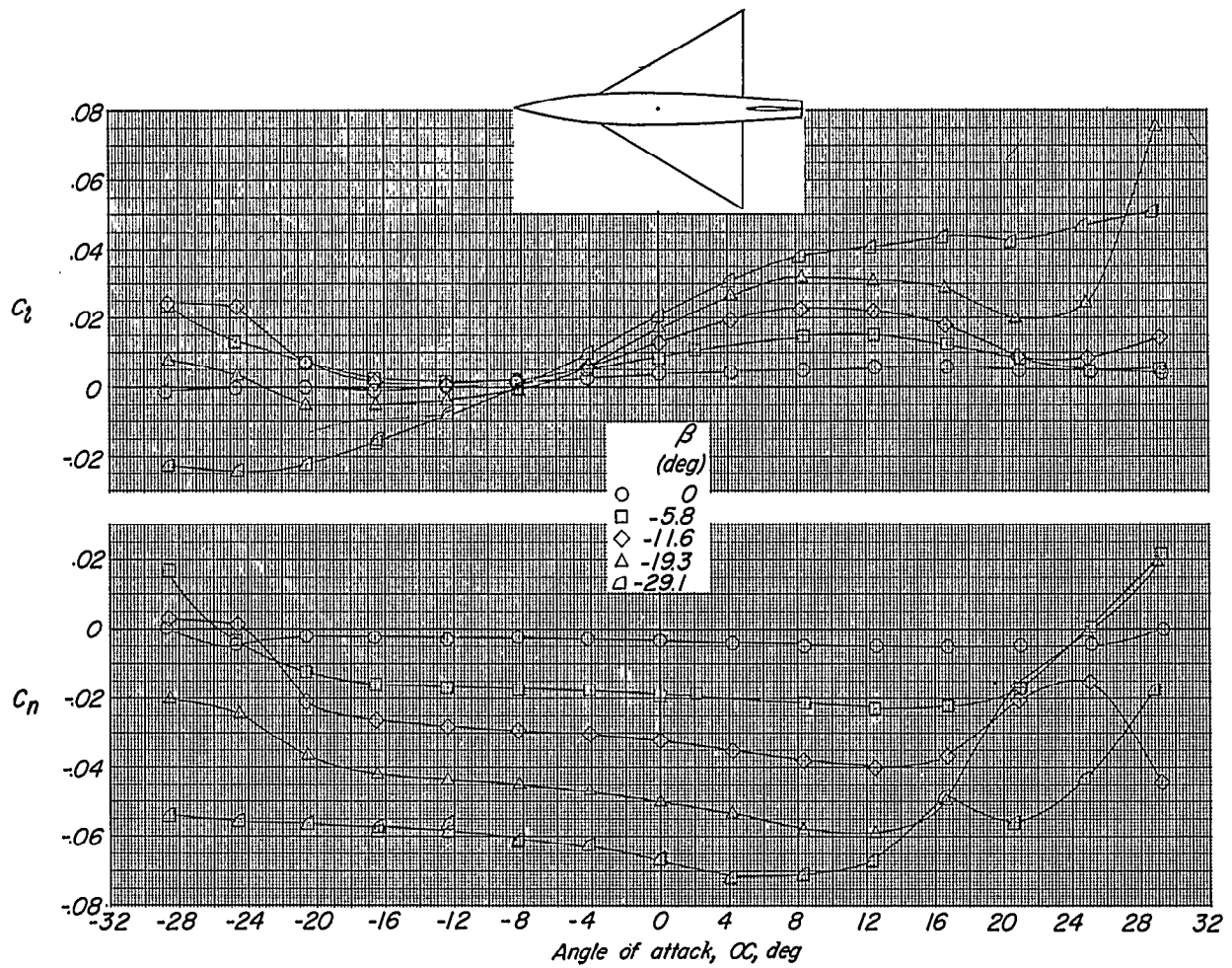

(c) C_l and C_n plotted against α.

Figure 6.- Concluded.

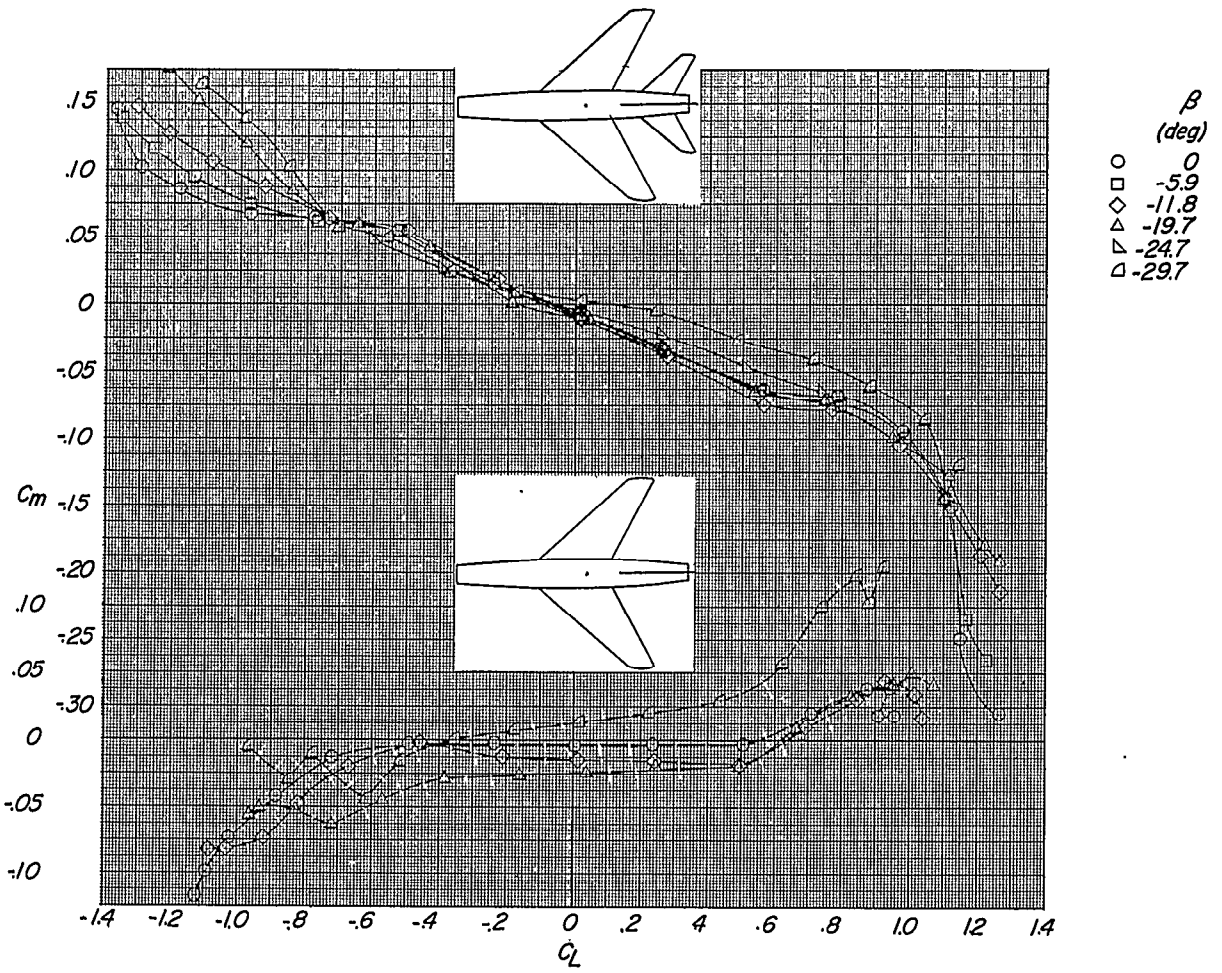

(a) Model A with $(i_t = 0^\circ)$ and without horizontal tail.

Figure 7.- Effect of sideslip angle on the variation of C_m with C_L for three fighter-type airplane models.

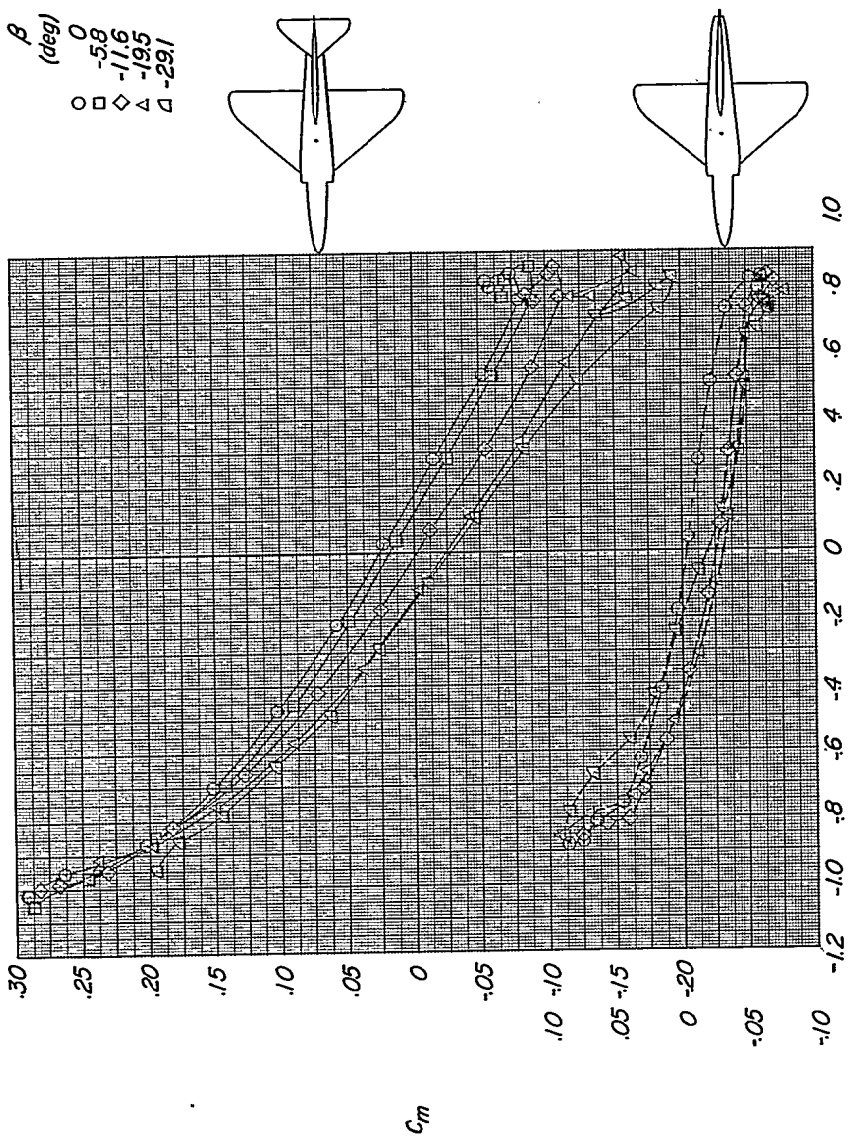

(b) Model B with $(i_t = 0^\circ)$ and without horizontal tail.

Figure 7.- Continued.

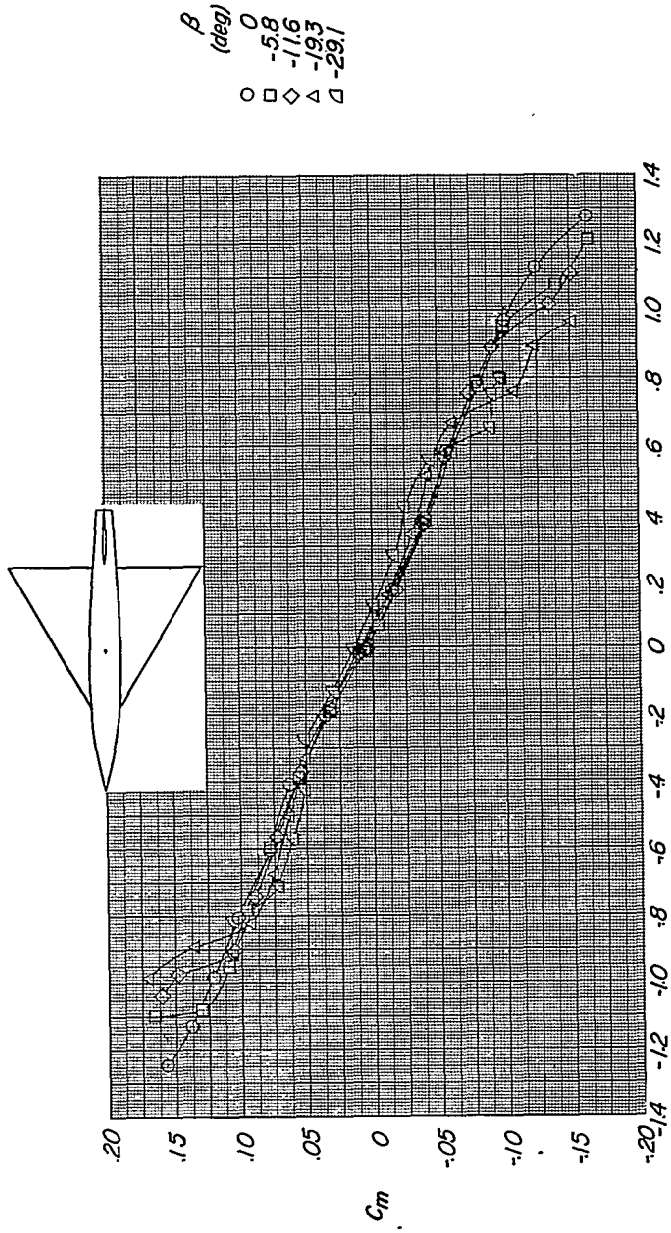

(c) Model C.

Figure 7.- Continued.

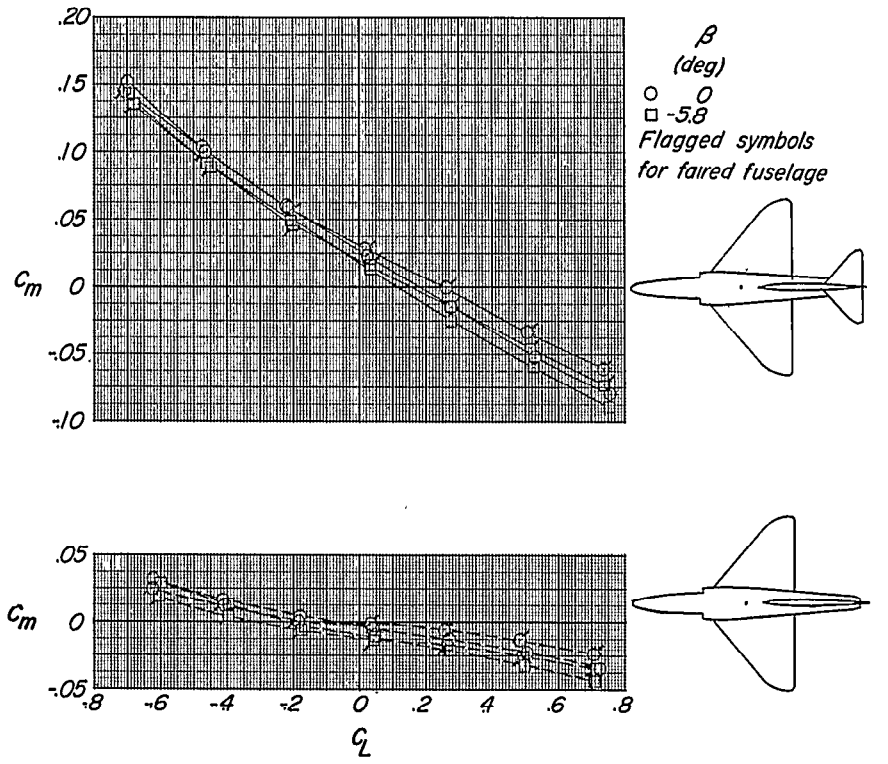

(d) Model B with $(i_t = 0^o)$ and without horizontal tail. Original and faired fuselage.

Figure 7.- Concluded.

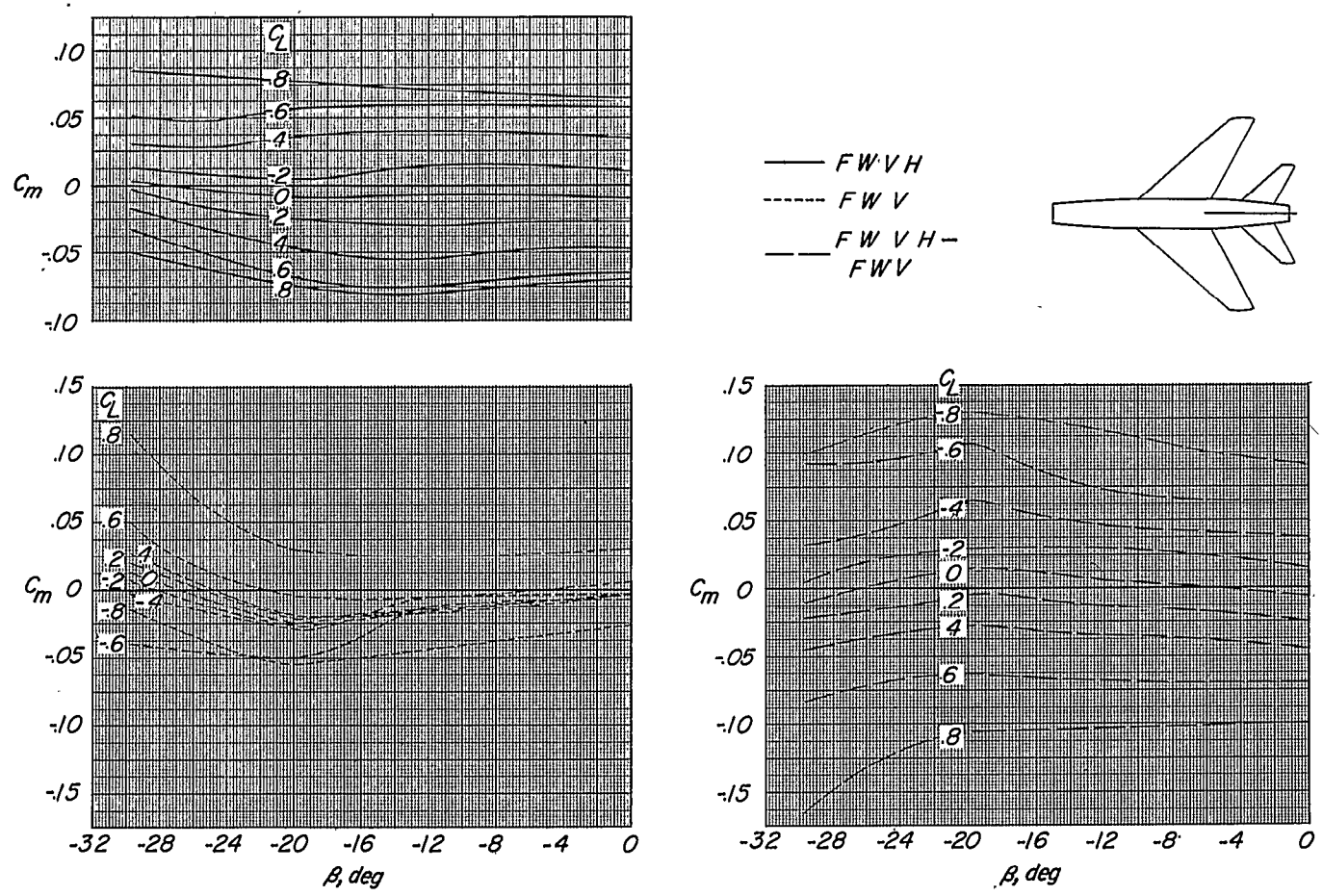

(a) Variation of C_m with β for complete model A $(i_t = 0°)$, complete model A less horizontal tail, and for horizontal-tail contribution.

Figure 8.- Effect of sideslip angle at several lift coefficients on pitching-moment coefficient of three fighter-type airplane models.

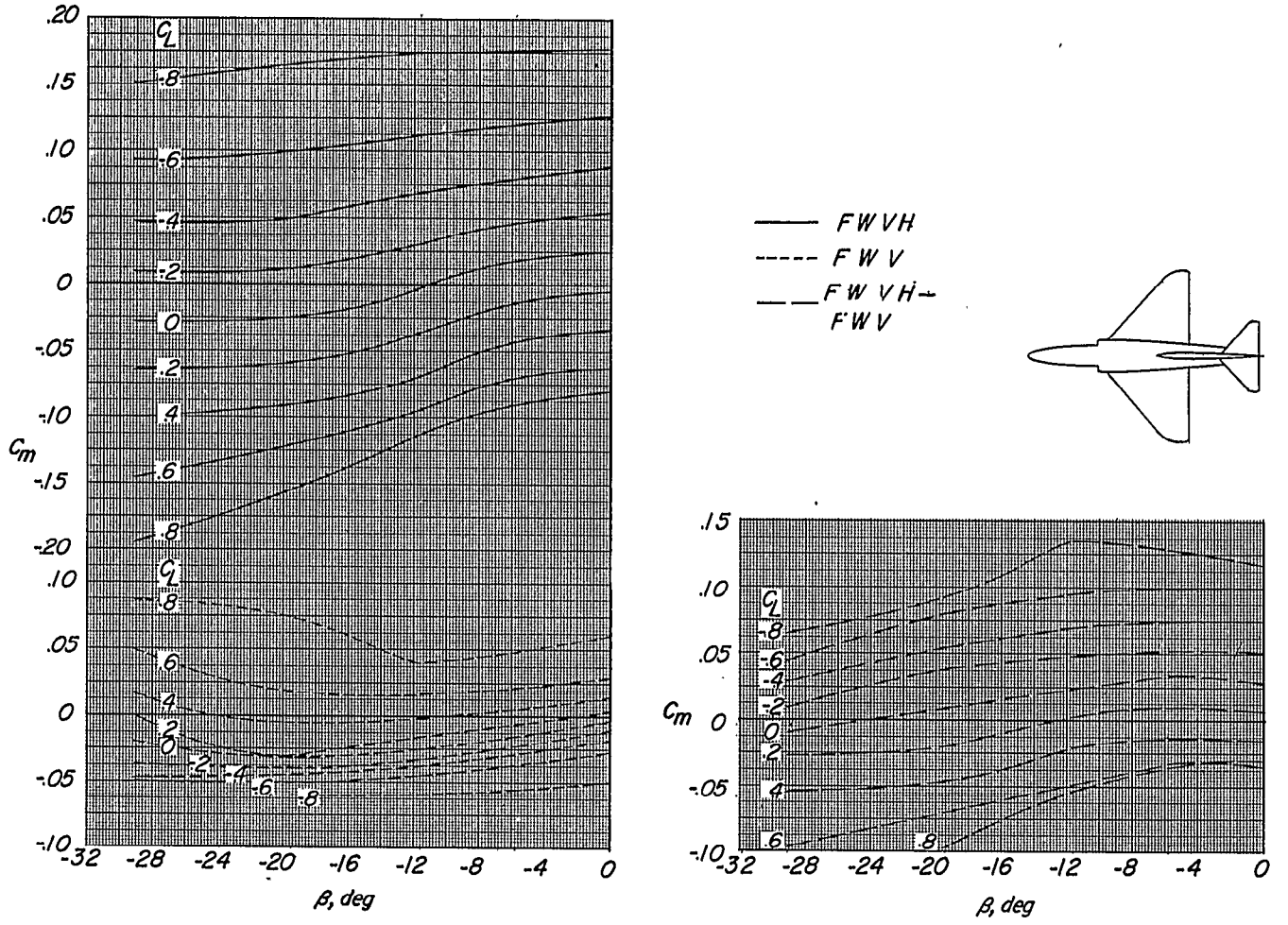

(b) Variation of C_m with β for complete model B $\left(i_t = 0^\circ\right)$, complete model B less horizontal tail, and for horizontal-tail contribution.

Figure 8.- Continued.

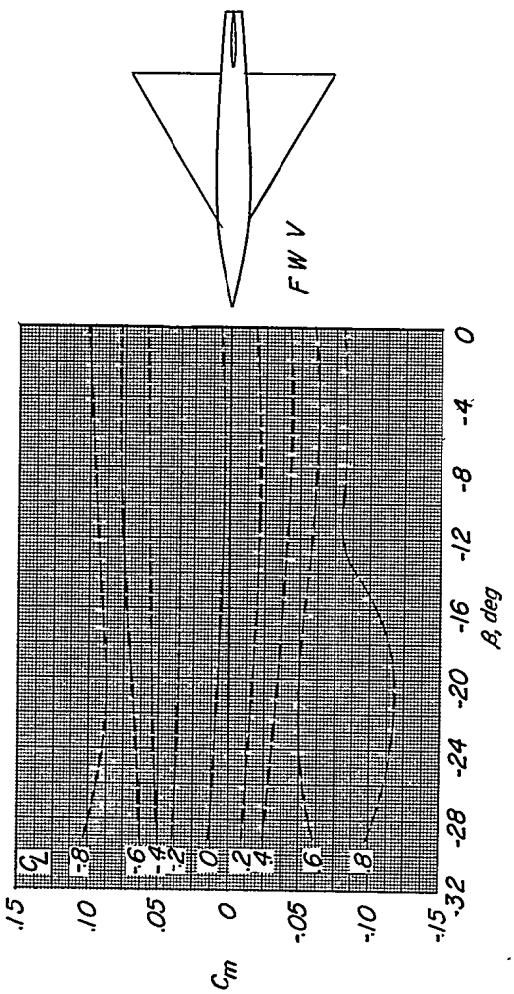

(c) Variation of C_m with β for model C.

Figure 8.- Concluded.

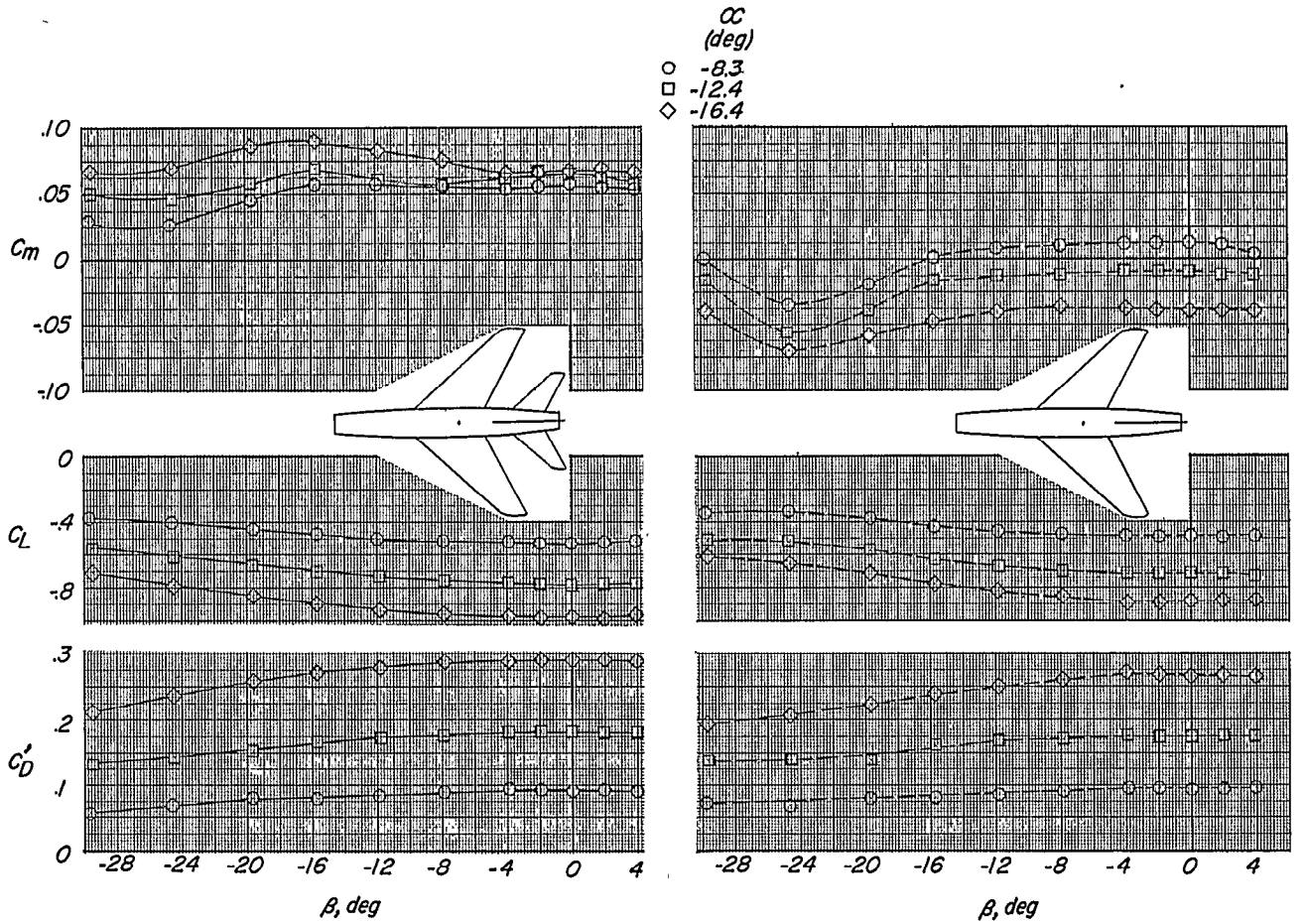

(a) Variation of C_m, C_L, and C_D' with β. Horizontal tail on $(i_t = 0^o)$ and off.

Figure 9.- Variation of aerodynamic characteristics with angle of sideslip for three angles of attack for model A.

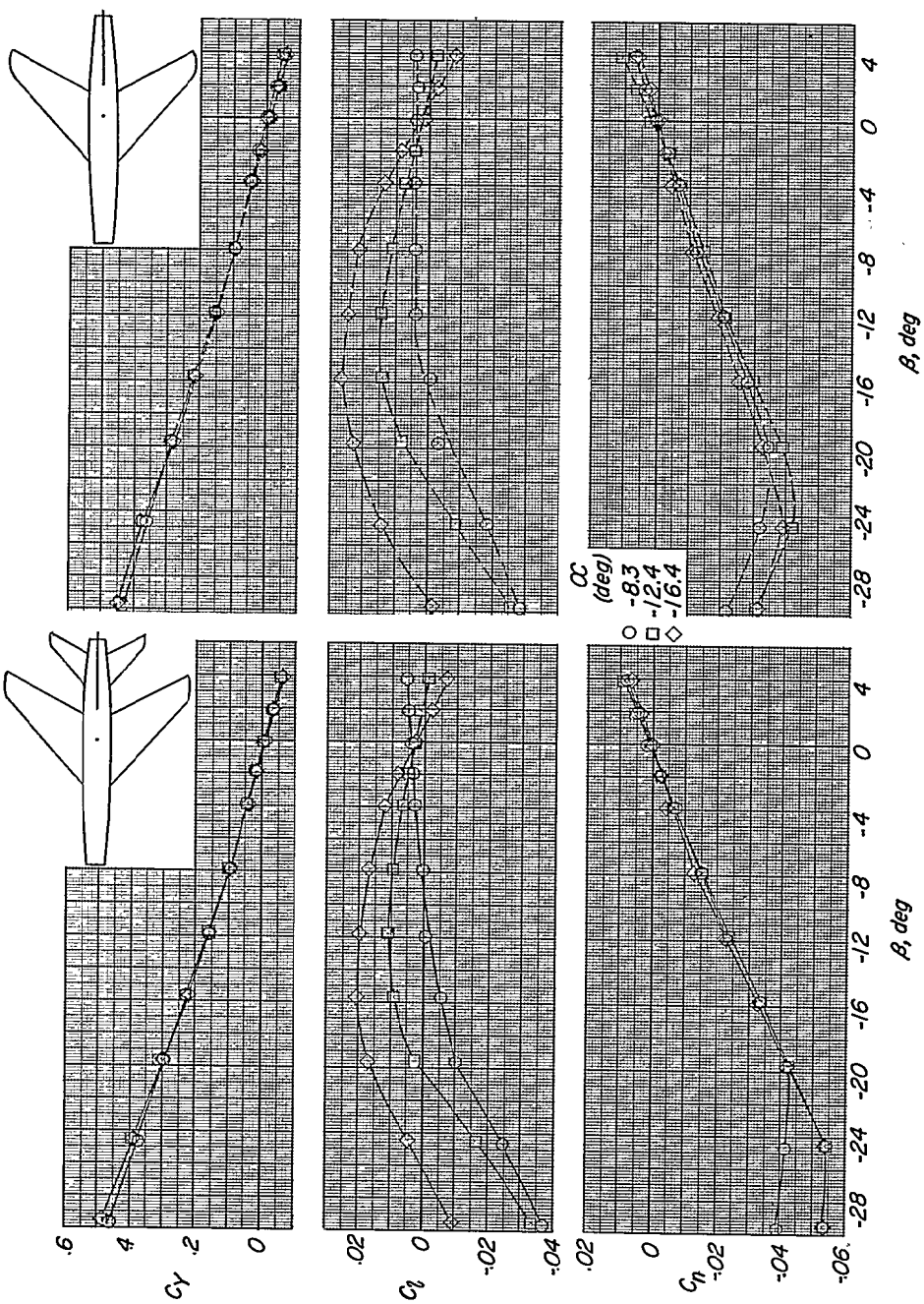

(b) Variation of C_Y, C_l, and C_n with β. Horizontal tail on $\left(i_t = 0^\circ\right)$ and off.

Figure 9.- Concluded.

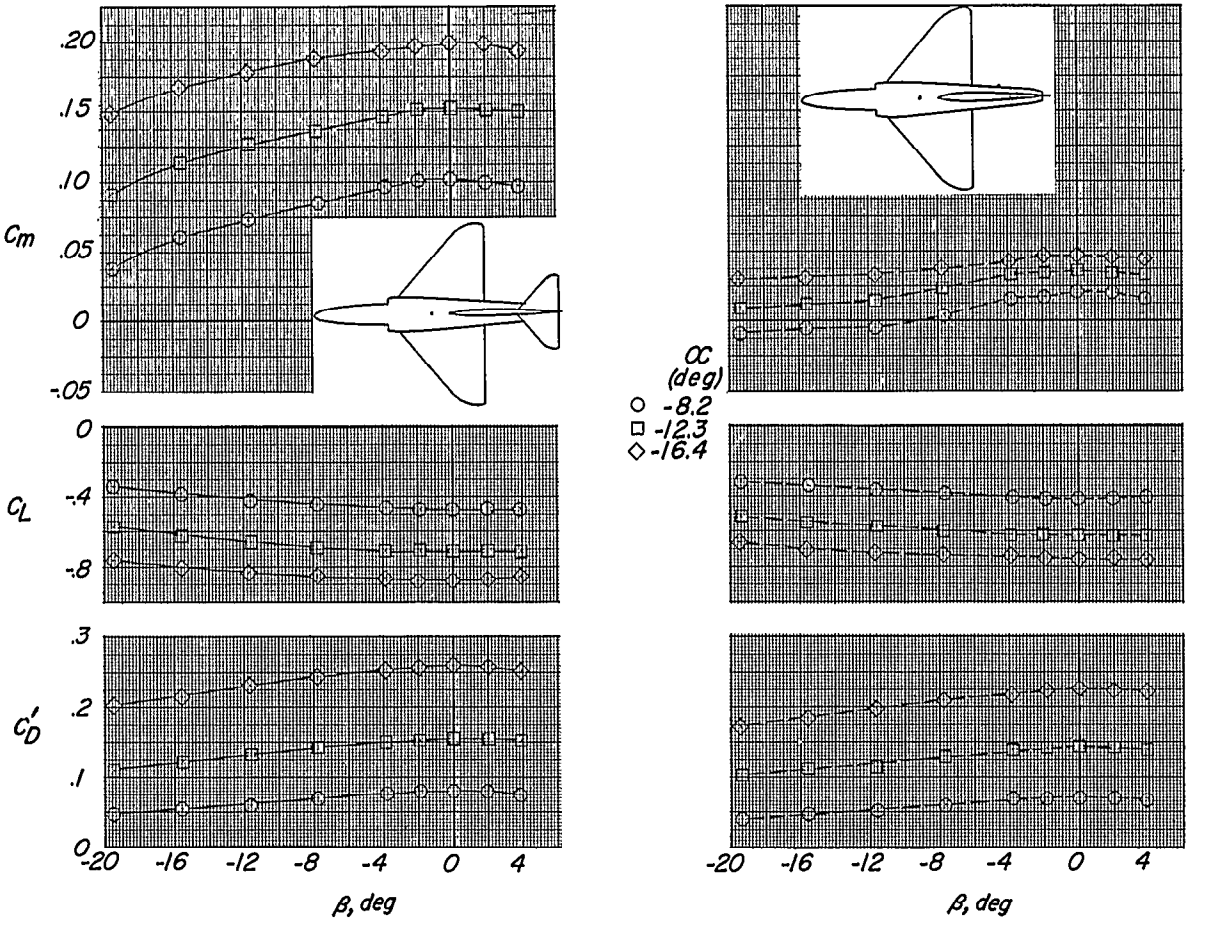

(a) Variation of C_m, C_L, and C'_D with β. Horizontal tail on $\left(i_t = 0^\circ\right)$ and off.

Figure 10.- Variation of aerodynamic characteristics with angle of sideslip for three angles of attack for model B.

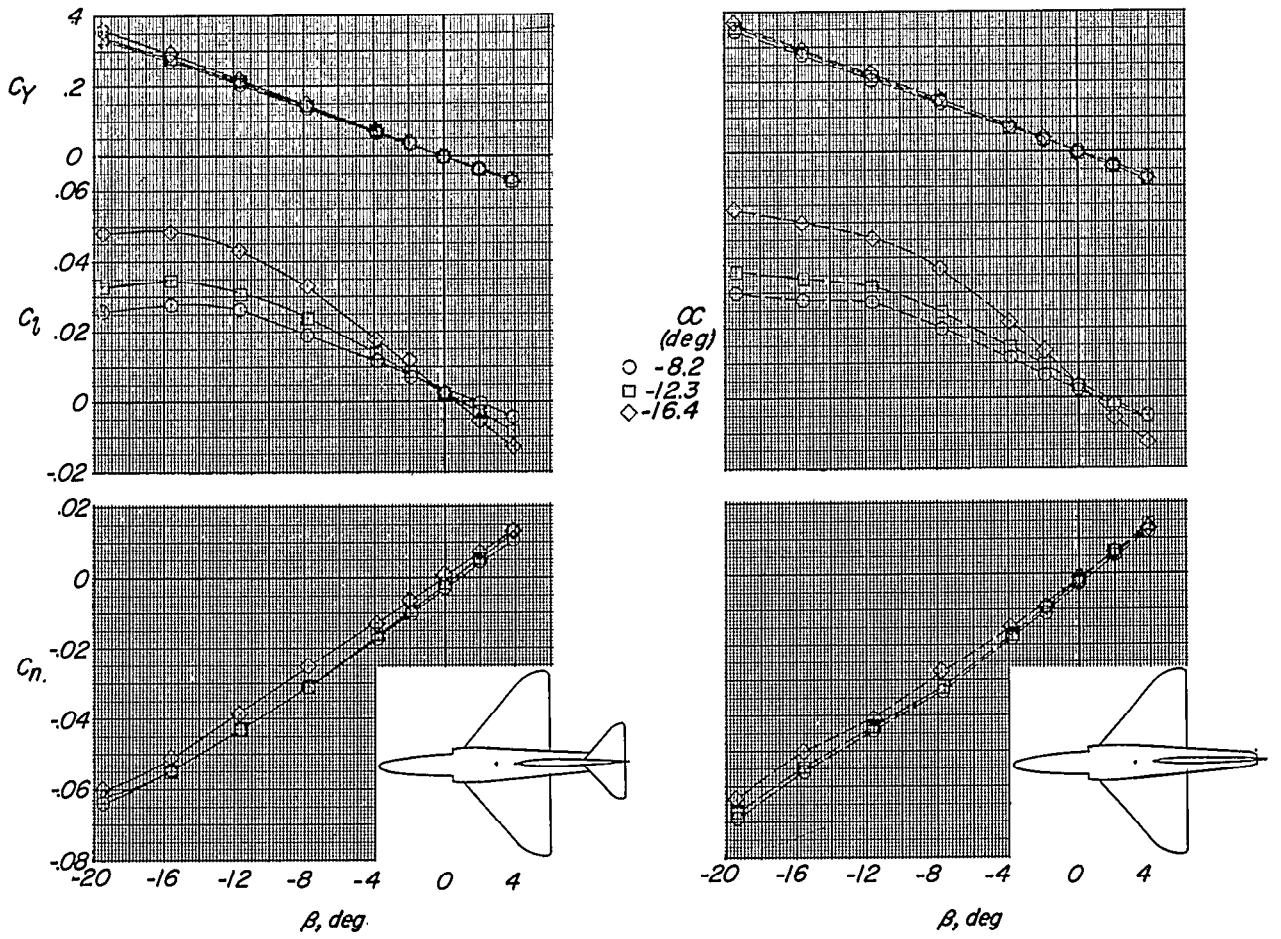

(b) Variation of C_Y, C_l, and C_n with β. Horizontal tail on $(i_t = 0^\circ)$ and off.

Figure 10.- Concluded.

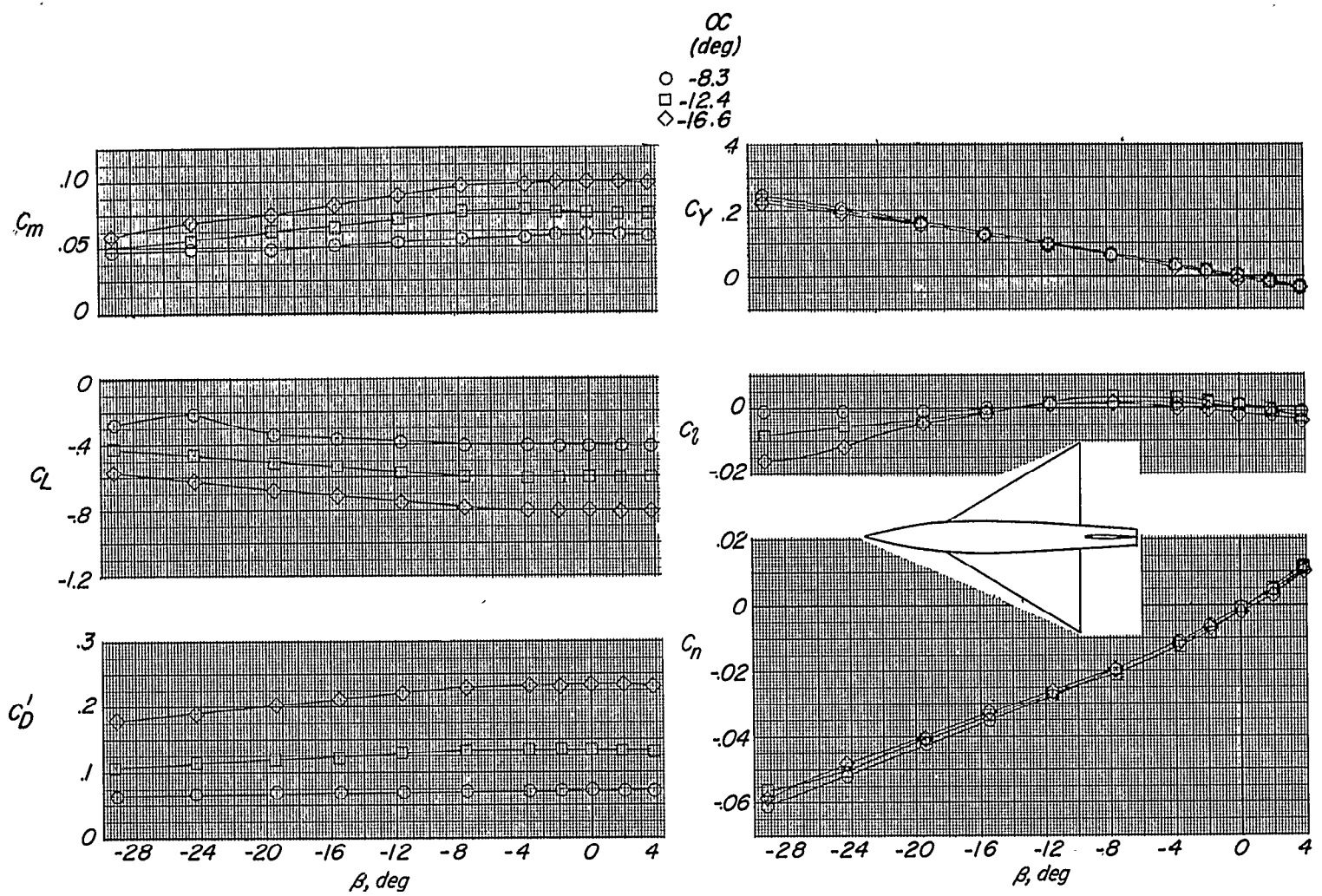

Figure 11.- Variation of aerodynamic characteristics with angle of sideslip for three angles of attack for model C.

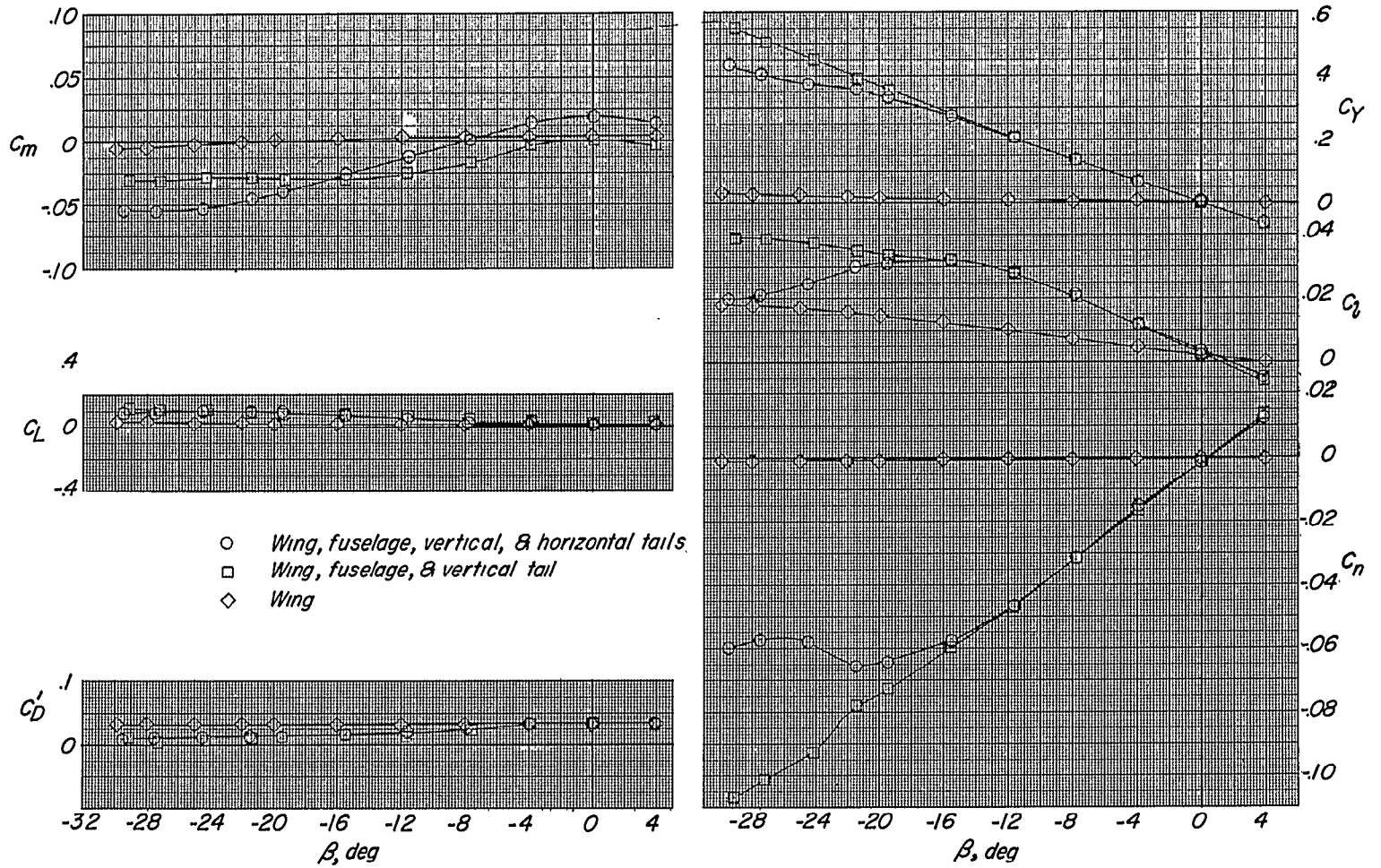

Figure 12.- Variation of aerodynamic characteristics with angle of sideslip for various components of model B. Original fuselage; $i_t = 0^\circ$; $\alpha = 0^\circ$.

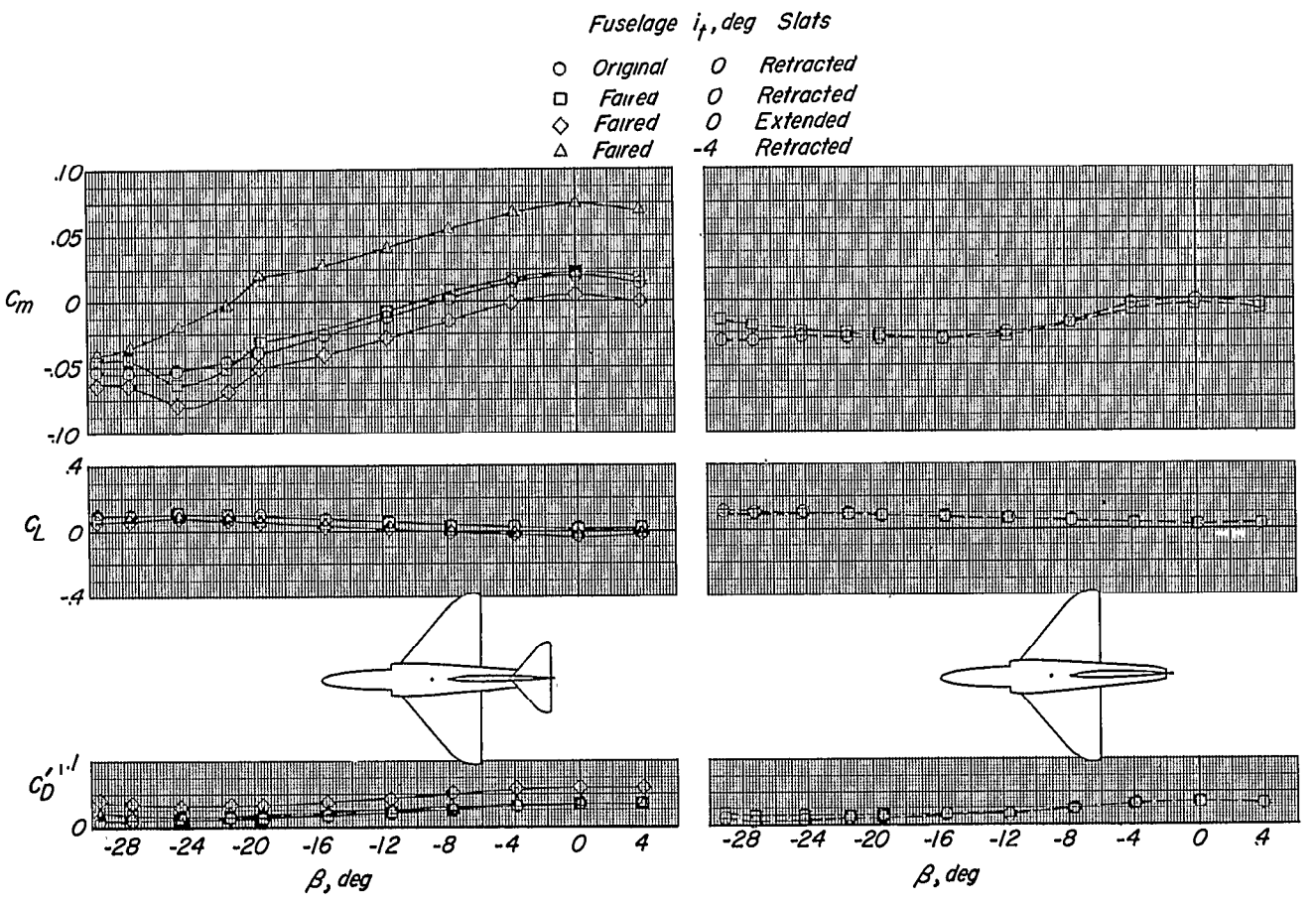

(a) Variation of C_m, C_L, and C_D' with β.
Horizontal tail on and off.

Figure 13.- Effect of fuselage fairing, slats, and horizontal-tail incidence on the variation of aerodynamic characteristics of model B with sideslip angle. $\alpha = 0^\circ$.

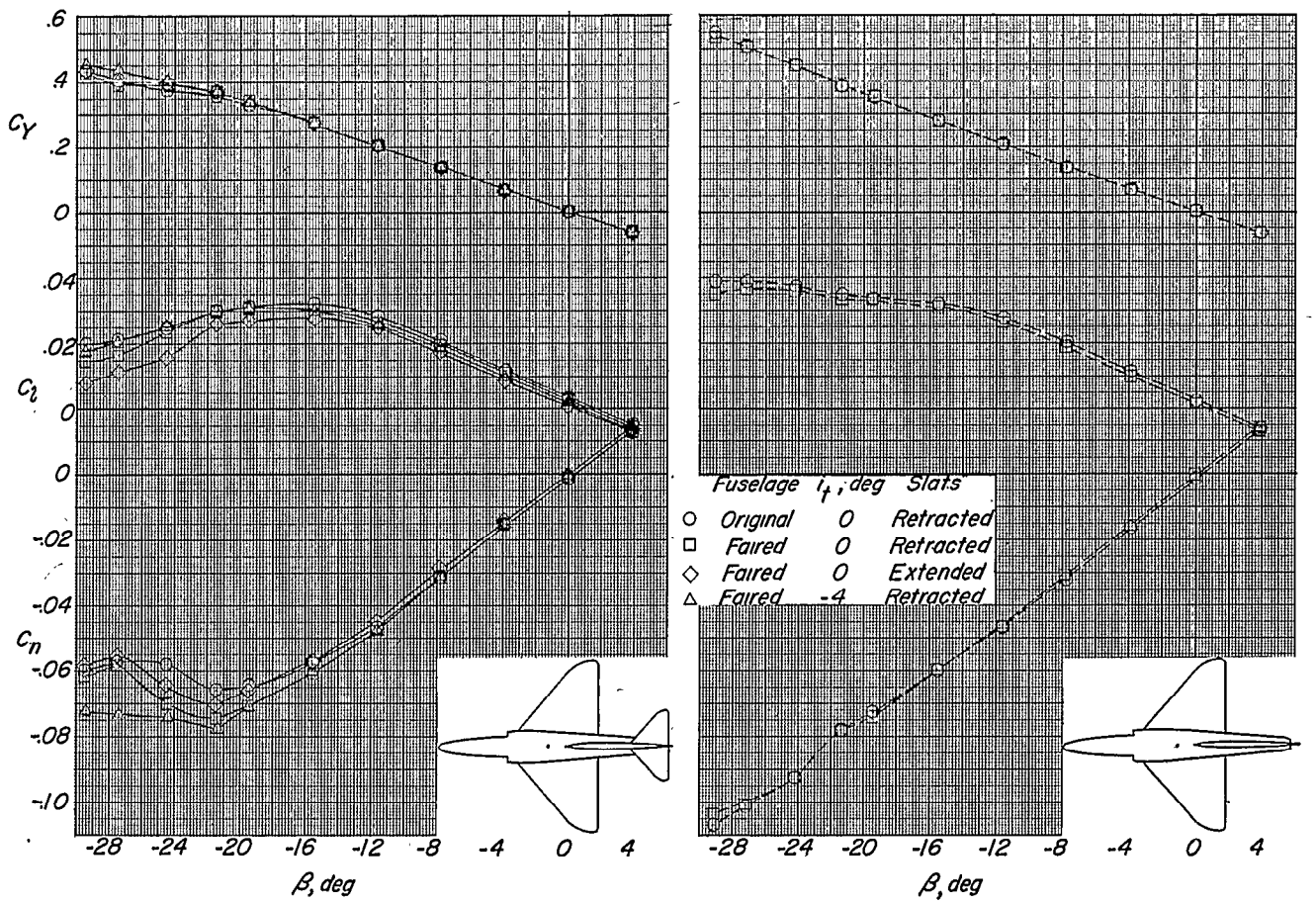

(b) Variation of C_Y, C_l, and C_n with β.
Horizontal tail on and off.

Figure 13.- Concluded.